Probabilistic Modeling of Hurricane Wind-Induced Damage in Infrastructure Systems

Derek Chang, Kerry Emanuel, and Saurabh Amin

Massachusetts Institute of Technology

Abstract

This paper presents a modeling approach for probabilistic estimation of hurricane wind-induced damage to infrastructural assets. In our approach, we employ a Nonhomogeneous Poisson Process (NHPP) model for estimating spatially-varying probability distributions of damage as a function of hurricane wind field velocities. Specifically, we consider a physically-based, quadratic NHPP model for failures of overhead assets in electricity distribution systems. The wind field velocities are provided by Forecasts of Hurricanes using Large-Ensemble Outputs (FHLO), a framework for generating probabilistic hurricane forecasts. We use FHLO in conjunction with the NHPP model, such that the hurricane forecast uncertainties represented by FHLO are accounted for in estimating the probability distributions of damage. Furthermore, we evaluate the spatial variability and extent of hurricane damage under key wind field parameters (intensity, size, and asymmetries). By applying our approach to prediction of power outages (loss-of-service) in northwestern Florida due to Hurricane Michael (2018), we demonstrate a statistically significant relationship between outage rate and failure rate. Finally, we formulate parametric models that relate total damage and financial losses to the hurricane parameters of intensity and size. Overall, this paper's findings suggest that our approach is well-suited to jointly account for spatial variability and forecast uncertainty in the damage estimates, and is readily applicable to prediction of system loss-of-service due to the damage.

Keywords: Hurricane Wind Risk, Infrastructural Damage, Probabilistic Modeling, Poisson Process, Outage Prediction

1 INTRODUCTION

Hurricanes are becoming an increasingly critical threat to infrastructure systems, especially as the destructive potential of hurricanes is expected to increase due to global warming (Emanuel, 2005). Climate simulations of hurricanes indicate that if little is done to curb greenhouse gas emissions and the world warms by 3-4°C this century, then hurricane rainfall will increase up to a third while wind intensity will be boosted by as much as 25 knots (Patricola & Wehner, 2018). The deleterious effects of hurricanes on infrastructure systems were highlighted in 2017 when electric power utilities struggled to handle the aftermath of Hurricanes Harvey, Irma, and Maria. Infrastructural vulnerability to hurricanes is further heightened by aging of critical infrastructure assets, as well as increasing coastal populations and development.

Effective post-hurricane infrastructure response and recovery strategies require accurate estimation of risk, or expected cost incurred due to hurricane-induced damage to the infrastructure. Broadly speaking, one computes risk by integrating the cost associated with infrastructural loss-of-service induced by various damage scenarios, over the probabilities of these scenarios. Generalized linear or additive regression models are commonly used to predict outages (i.e., loss-of-service) (Liu, Davidson, Rosowsky, & Stedinger, 2005; Liu, Davidson, & Apanasovich, 2007; Han et al., 2009) in electric power infrastructure, as a function of parameters related to the hurricane's physical structure and the local environment. However, these models do not generate probabilistic, spatially-varying predictions of damage to infrastructure assets. A lack of adequate damage predictions impedes pre-storm resource allocation, warehouse selection, vehicle fleet routing, damage localization, and repair operations (Van Hentenryck, Bent, & Coffrin, 2010; Lee, Dahan, Weinert, & Amin, 2019). Slow damage localization and repair result in an increased time duration during which the infrastructure fails to adequately provide service to end-users.

In this article, we focus on modeling of hurricane wind-induced damage to overhead infrastructural assets. The damages are dependent on hurricane wind characteristics such as local wind speed, direction, and duration, which are functions of the hurricane track and intensity. The hurricane track forecast is typically provided by the National Hurricane Center (NHC) hour/days ahead of the hurricane's forecasted landfall. Forecasts provide estimated future locations of the hurricane eye (center) at discrete time steps (3-6 hour intervals are typical). The NHC forecast also includes track uncertainty estimates in the form of a 'cone of uncertainty', which surrounds the forecasted track and

represents the probable trajectories that the hurricane may take.[1] In recent history, the realized hurricane track fell within the cone about 60-70% of the time (Center, n.d.). This suggests that the temporal evolution of the hurricane track is highly uncertain. Ensemble prediction systems have the potential to significantly improve probabilistic forecasts of hurricanes by accounting for real-time uncertainties (Majumdar & Finocchio, 2010; Hamill, Whitaker, Fiorino, & Benjamin, 2011; Lin, Emanuel, & Vigh, 2020) (see Figure 1a).

The hurricane intensity is typically computed by models such as the Coupled Hurricane Intensity Prediction System (CHIPS) (Emanuel, DesAutels, Holloway, & Korty, 2004) or FAST intensity simulator (Emanuel, 2017). Then given a hurricane track and intensity, one can deduce wind velocities at arbitrary locations that may be affected by the storm, as given by a surface wind field.[2] The surface wind field is typically represented by fitting canonical radial wind distributions to the storm's forecast intensity and radius of maximum winds (see Figure 1b). Most parametric wind field models are axisymmetric, i.e., wind velocities are assumed to be equal at equidistant locations from the storm center (Holland, 1980; Vickery, Skerlj, Steckley, & Twisdale, 2000; Emanuel, 2004; Vickery, Wadhera, Powell, & Chen, 2009; Chavas, Lin, & Emanuel, 2015). On the other hand, asymmetric wind field models (Xie, Bao, Pietrafesa, Foley, & Fuentes, 2006; Chang, Amin, & Emanuel, 2020) account for wind variability with respect to both radial distance and azimuthal angle.[3]

Here, we formulate a damage modeling approach that bridges the existing gap in the application of hurricane models and forecasting methods (Holland, 1980; Vickery et al., 2000; Emanuel, 2004; Emanuel et al., 2004; Xie et al., 2006; Vickery et al., 2009; Majumdar & Finocchio, 2010; Hamill et al., 2011; Chavas et al., 2015; Emanuel, 2017; Chang, Amin, & Emanuel, 2020; Lin et al., 2020) to damage estimation. Our probabilistic modeling approach accounts for the effects of both hurricane forecast uncertainty and spatial variability in wind velocities (see Section 2). To represent the uncertainty in the forecasted hurricane's temporal evolution, we employ "Forecasts of Hurricanes using Large-Ensemble Outputs" (FHLO), which produces 1,000-member forecast track and intensity ensembles (Lin et al., 2020). To incorporate the effect of spatially-varying wind velocities, we employ a physically-based Nonhomogeneous Poisson Process (NHPP) model (Brown, Gupta, Christie, Venkata, & Fletcher, 1997; Zhou, Pahwa, & Yang, 2006; Alvehag & Söder, 2011; Li et al., 2014) for probabilistic damage estimation. The NHPP model outputs spatially-

---

[1] To form the cone of uncertainty, one estimates the uncertainty in the forecasted track location at each discrete time step. The uncertainty at a time step is represented by a circle that surrounds the forecasted track location associated with this time. The union of the circles is the cone of uncertainty, and the cone shape reflects increasing uncertainty with time.

[2] Most wind field models estimate 1- or 10-minute sustained winds.

[3] The difference between the highest and lowest velocities around the radius of maximum winds can readibly be around 10 m/s (Uhlhorn, Klotz, Vukicevic, Reasor, & Rogers, 2014).

varying probability distributions of the extent of damage (number of asset failures), using a hurricane wind forecast as input.

In Section 3, we provide an analysis of the formulated modeling approach. First, we define the "critical zone" or geographical region that suffers from hurricane wind-induced damage. Then, we assess how spatial variability in wind velocities and forecast uncertainty represented by FHLO impact the damage estimates. In Section 4, we apply our modeling approach to the prediction of outages (i.e., loss-of-service) in electric power infrastructure due to Hurricane Michael. In Section 5, we provide brief insights into how hurricane intensity and size impact total damage and resulting financial losses. Finally, we provide concluding remarks in Section 6.

2 MODELING APPROACH

In this section, we develop a probabilistic model for estimating spatially-varying damage to overhead assets in infrastructure systems. To evaluate damage due to hurricane winds, we estimate a probability distribution over the number of failed assets in each defined two-dimensional spatial region $g \in \mathcal{G}$. In our approach, the location-specific probability distribution is dependent on the hurricane surface wind field velocities, which are forecasted at each location $g \in \mathcal{G}$ and time $t \in \mathcal{T}$. The set of times $\mathcal{T}$ encompasses discrete time steps between the initial forecast time t_0 and final forecast time t_{f}, where forecast duration $\mathrm{T} = t_{\mathrm{f}} - t_0$. The times are equally spaced and separated by a time interval of Δt.

We use $\mathbf{H} = \{v_{g,t}\}_{g \in \mathcal{G}, t \in \mathcal{T}}$ to denote the hurricane wind field as a random field, where $v_{g,t}$ defines the velocity at location g and time t. Furthermore, $\mathbf{H}_g = \{v_{g,t}\}_{t \in \mathcal{T}}$ denotes the velocities corresponding to location g, and $\mathbf{H}_t = \{v_{g,t}\}_{g \in \mathcal{G}}$ the velocities corresponding to time t. Henceforth, we will use the notation $\tilde{\mathbf{H}}$ to denote a specific instance of a hurricane wind field, which can be appropriately subscripted using g and t.

The probabilistic hurricane surface wind field forecast is given by Forecasts of Hurricanes using Large-Ensemble Outputs (FHLO), which we discuss in Section 2.1. Using a surface wind field forecast (FHLO) as input, we estimate probability distributions of damage (number of failed assets) within the infrastructure system by employing the nonhomogeneous Poisson Process (NHPP) model (Section 2.2). Finally, we discuss how the NHPP model can be integrated with FHLO, in order to account for forecast uncertainties in damage estimates (see Section 2.3).

2.1 Forecasts of Hurricanes using Large-Ensemble Outputs (FHLO)

Forecasts of Hurricanes using Large-Ensemble Outputs (FHLO) is a physically-based model framework developed by Lin, Emanuel, and Vigh (Lin et al., 2020), which generates probabilistic forecasts of the hurricane wind field. Specifically, FHLO is used to produce probability distributions of wind velocity at fixed locations in space, using a three-component framework: 1) a track model that bootstraps 1,000 synthetic tracks from the much smaller number of forecast hurricane tracks from an ensemble numerical weather prediction model; 2) an intensity model that predicts the maximum wind speed along each synthetic track; and 3) a parametric wind field model that estimates the time-varying two-dimensional surface wind field along each synthetic track given the position and intensity of the storm. We use $\mathcal{H} = \{\tilde{\mathbf{H}}^{(i)}\}_{\forall i \in \{1,\dots,H\}}$ to refer to a hurricane ensemble obtained from FHLO: the ensemble consists of $H = 1,000$ ensemble members, where each member is indexed by i and denoted by $\tilde{\mathbf{H}}^{(i)} = \{v_{g,t}^{(i)}\}_{g \in \mathcal{G}, t \in \mathcal{T}}$. The empirical probability of the wind field $\tilde{\mathbf{H}}^{(i)}$ is $1/H$.

FHLO assumes an initialization time at which the forecast begins, typically 1-3 days before the hurricane is projected to make landfall. Randomness in hurricane tracks and wind velocities stems from forecast uncertainty in the hurricane track evolution, dynamic and thermodynamic environments, and initial conditions. The probabilistic intensity forecasts given by FHLO are comparable in accuracy to those of the Hurricane Weather Research and Forecasting (HWRF) model, an advanced numerical weather prediction model, but also far less computationally intensive to produce.

2.2 Nonhomogeneous Poisson Process (NHPP) Model

We now focus on generating probabilistic, spatially-varying estimates of damage, using a hurricane wind field $\tilde{\mathbf{H}}$ as input. For each spatial location $g \in \mathcal{G}$, we aim to compute a probability distribution over the number of damaged assets in g accumulated over the set of times $t \in \mathcal{T}$. To compute the probability distributions, we employ a Nonhomogeneous Poisson Process (NHPP) model, in which the rate of failures is time-varying to reflect the dependence of infrastructural asset failures on the hurricane wind velocities.

The NHPP model is used to estimate the Poisson intensities $\lambda_{g,t}$ for locations $g \in \mathcal{G}$ and at times $t \in \mathcal{T}$. The Poisson intensity is the expected number of failures per unit time, normalized by the asset density. We model the Poisson intensity $\lambda_{g,t}$ to be a function of the velocity $v_{g,t}$; the parametric form of the function depends on the

infrastructure system and asset type in question. The Poisson intensities $\lambda_{g,t}(v_{g,t})$ for $t \in \mathcal{T}$ can be used to compute the failure rate Λ_g, the expected number of failures in g accumulated over the hurricane's lifetime and normalized by the asset density:

$$\Lambda_g(\mathbf{H}_g) \;=\; \sum_{t \in \mathcal{T}} \lambda_{g,t}(v_{g,t})\, \Delta t, \tag{1}$$

where Δt is the time spacing between each time $t \in \mathcal{T}$. A typical measure of Δt is one hour.

Both the Poisson intensity and failure rate are measures of expected damage when the number of assets per location can be treated as a large number (infinite). Under this assumption, the probability that there are s_g failures in location g, normalized by asset density, is given by the Poisson distribution:

$$\Pr(s_g \mid \Lambda_g) \;=\; \frac{\Lambda_g^{s_g}}{s_g!}\exp(-\Lambda_g), \tag{2}$$

where Λ_g, the failure rate, is also referred to as the Poisson parameter.

If the asset density l_g in g is known, then the corresponding "total" failure rate is $l_g\Lambda_g$. If we wish to obtain the distribution over the total number of failures (rather than normalized failures) in a location g, we use $l_g\Lambda_g$ as the Poisson parameter in place of Λ_g. In the example of electricity distribution lines, Λ_g would be the expected number of failures per kilometer of distribution lines and l_g is the length of distribution lines in kilometers within location g.

In reality, the number of assets per location is finite and varies across locations. If there are a finite number of assets $\bar{S}_g$ in a location g, then the distribution over the total number of failed assets must be modified accordingly:

$$\Pr(s_g \mid l_g\Lambda_g) \;=\;
\begin{cases}
\frac{(l_g\Lambda_g)^{s_g}}{s_g!}\exp(-l_g\Lambda_g), & \text{for } s_g < \bar{S}_g \\[2mm]
1 - \exp(-l_g\Lambda_g)\sum_{x=0}^{\bar{S}_g-1}\frac{(l_g\Lambda_g)^x}{x!}, & \text{for } s_g = \bar{S}_g
\end{cases} \tag{3}$$

Hereafter, we refer to the distribution given by Eq. (3) as incorporating "saturation" in the number of failures. Under this distribution, the expected number of failures $\mathbb{E}[s_g]$ normalized by asset density is not given by $\bar{S}_g\Lambda_g$, but rather by:

$$
\begin{aligned}
\mathbb{E}[s_g] \;&=\; \sum_{x=0}^{\bar{S}_g} x\,\Pr(s_g = x) \;=\; \sum_{x=0}^{\bar{S}_g-1} x\,\frac{(l_g\Lambda_g)^x}{x!}\exp(-l_g\Lambda_g) + \bar{S}_g\left[1 - \exp(-l_g\Lambda_g)\sum_{x=0}^{\bar{S}_g-1}\frac{(l_g\Lambda_g)^x}{x!}\right] \\[2mm]
&=\; l_g\Lambda_g\exp(-l_g\Lambda_g)\sum_{x=1}^{\bar{S}_g-1}\frac{(l_g\Lambda_g)^{x-1}}{(x-1)!} + \bar{S}_g\left[1 - \exp(-l_g\Lambda_g)\sum_{x=0}^{\bar{S}_g-1}\frac{(l_g\Lambda_g)^x}{x!}\right],
\end{aligned} \tag{4}
$$

where $\Pr(s_g = x)$ is the probability of x events as given by the Poisson distribution in Eq. (3). Figure 2 demonstrates

how incorporating saturation affects the expected number of failures $\mathbb{E}[s_g]$ in a location g, following Eq. (4). Notice that $\mathbb{E}[s_g]$ asymptotically approaches $\bar{S}$, the total number of assets in g. In this case we consider a location with $\bar{S}_g = 30$ distribution lines (3 kilometers of lines in the location, where each line has a length of 100 meters).

In this work, we focus on an NHPP model for hurricane wind-induced failures of overhead infrastructural assets in electricity distribution systems. In particular, failures of electricity distribution lines are a frequent cause of outages in power systems (Campbell, 2013), and typically result from downing of supporting poles or toppling by nearby trees. A standard means of modeling the Poisson intensity for failure of overhead assets is to use a quadratic function (Brown et al., 1997; Alvehag & Söder, 2011; Li et al., 2014) or exponential function (Lallemand, 2008). In this work, we focus on a quadratic model for Poisson intensity $\lambda_{g,t}$, the expected number of failures per hour and kilometer of assets (i.e., distribution lines):

$$\lambda_{g,t}(v_{g,t}) = \begin{cases} \left(1 + \alpha\left(\left(\frac{v_{g,t}}{V_{\text{crit}}}\right)^2 - 1\right)\right)\lambda_{\text{norm}}, & \text{if } v_{g,t} \geqslant V_{\text{crit}} \\ \lambda_{\text{norm}}, & \text{if } v_{g,t} < V_{\text{crit}}. \end{cases} \tag{5}$$

A quadratic function reflects the fact that the pressure exerted on trees and poles is a function of the wind velocity squared. The model's key physically-based feature is the quadratic relationship between $\lambda_{g,t}$ and $v_{g,t}$ when $v_{g,t}$ is greater than the so-called critical velocity V_{crit}. For velocities below V_{crit}, the infrastructure system only suffers from a fixed nominal failure rate of λ_{norm}.[4] The parameter α is a scaling parameter that controls for the increase in failure rate with velocities above V_{crit}. All three model parameters (V_{crit}, λ_{norm}, and α) are dependent on the asset type and properties (i.e., height, age, material composition). For the remainder of this article, we use the following parameter values (adapted from (Li et al., 2014)): $V_{\text{crit}} = 20.6$ m/s, $\alpha = 4175.6$, and $\lambda_{\text{norm}} = 3.5 \times 10^{-5}$ failures/hr/km.[5]

The equation can be rewritten accordingly, to separate the constant term and velocity-dependent term:

$$\lambda_{g,t}(v_{g,t}) = \lambda_{\text{norm}}(1 - \alpha) + \lambda_{\text{norm}}\alpha f^2(v_{g,t}), \tag{6}$$

where

$$f(v_{g,t}) = \frac{\max(V_{\text{crit}}, v_{g,t})}{V_{\text{crit}}}. \tag{7}$$

---

[4]Literature has suggested that V_{crit} is 8 m/s, when using historical Swedish weather data in which velocities did not exceed 20 m/s (Alvehag & Söder, 2011), In contrast, V_{crit} was estimated to be 20.6 m/s when using velocities from historical hurricanes up to Category 2 intensity on the Saffir-Simpson scale (Li et al., 2014).

[5]Other considerations such as precipitation and soil cover have also been shown to be relevant to modeling of failures and outages, but we focus solely on the variability of Poisson intensities due to the hurricane wind velocities.

Using Eq. (1), the failure rate Λ_g for all $g \in \mathcal{G}$ is given by:

$$\Lambda_g(\mathbf{H}_g) \;=\; \lambda_{\text{norm}} \mathrm{T}(1 - \alpha) \;+\; \lambda_{\text{norm}} \alpha \Delta t \sum_{t \in \mathcal{T}} f^2(v_{g,t}). \tag{8}$$

Previous applications of the presented quadratic model (Zhou et al., 2006; Alvehag & Söder, 2011; Li et al., 2014) did not evaluate the spatial variability in estimated Poisson failure rates due to the physical structure of the hurricane wind field, even though hurricane wind velocities vary significantly with space and time. In contrast, our approach incorporates spatiotemporal variabilities in winds to estimate the Poisson failure rates. We are also readily able to replace the quadratic model with an exponential model for the Poisson intensity within the modeling approach. Furthermore, it is worth noting that our estimated failure rates use wind velocity inputs at one-hour intervals, as opposed to intervals of 3+ hours in the abovementioned applications of the quadratic model.

In Section 4, we will discuss how saturation in Eq. (3)-(4) and the critical velocity parameter in Eq. (5) are reflected in outages resulting from Hurricane Michael.[6] We note that a cubic function for the Poisson intensity is suitable if the effects of blowing debris are considered (Emanuel, 2011). The effect of using different Poisson intensity functions could also possibly be examined using real-life failure or outage data.

2.3   Integrating FHLO and NHPP Model

We discuss how to incorporate hurricane forecast uncertainty, as given by FHLO, in estimating (i) failure rates and (ii) failure distributions using the quadratic NHPP model in Section 2.2. In contrast, previous works (Zhou et al., 2006; Alvehag & Söder, 2011; Li et al., 2014) did not incorporate hurricane forecast uncertainties in failure rate estimation, in addition to not analyzing how failure rates are affected by wind velocity variability.

First we define the expected velocity, denoted $\bar{v}_{g,t}$ in location g at time t, under a given hurricane ensemble $\mathcal{H}$ with H ensemble members:

$$\bar{v}_{g,t} \;=\; \mathbb{E}[v_{g,t}] \;=\; \frac{1}{\mathrm{H}} \sum_{i=1}^{\mathrm{H}} v_{g,t}^{(i)}, \tag{9}$$

where $v_{g,t}^{(i)}$ is the velocity in grid g at time t, for ensemble member i. For notational convenience, we use $\mathbb{E}[\mathbf{H}_g]$ to denote $\{\bar{v}_{g,t}\}_{t \in \mathcal{T}}$ and $\mathbb{E}[\mathbf{H}]$ to denote $\{\bar{v}_{g,t}\}_{g \in \mathcal{G}, t \in \mathcal{T}}$.

One can consider two ways to incorporate FHLO in estimating failure rates:

---

[6]It is also possible to account for saturation directly in the Poisson intensity function, rather than using Eq. (3)-(4).

- **Failure Rate 1 (FR-1)**: the failure rate as a function of the ensemble-averaged wind velocities, denoted by $\Lambda_g(\mathbb{E}[\mathbf{H}_g])$. Using Eq. (1), FR-1 for a location g can be written as:

$$\Lambda_g(\mathbb{E}[\mathbf{H}_g]) \;=\; \sum_{t \in \mathcal{T}} \lambda_{g,t}(\bar{v}_{g,t}) \Delta t. \tag{10}$$

Then, using Eq. (8), FR-1 under the quadratic NHPP model can be written as:

$$\Lambda_g(\mathbb{E}[\mathbf{H}_g]) \;=\; \lambda_{\text{norm}} T(1 - \alpha) \;+\; \lambda_{\text{norm}} \alpha \Delta t \sum_{t \in \mathcal{T}} f^2(\bar{v}_{g,t}). \tag{11}$$

- **Failure Rate 2 (FR-2)**: the ensemble-averaged failure rate, denoted by $\mathbb{E}[\Lambda_g(\mathbf{H}_g)]$. Using Eq. (1), FR-2 for a location g can be written as:

$$\begin{aligned}
\mathbb{E}[\Lambda_g(\mathbf{H}_g)] \;&=\; \frac{1}{\text{H}} \sum_{i=1}^{\text{H}} \Lambda_g(\tilde{\mathbf{H}}_g^{(i)}) \\
&=\; \frac{1}{\text{H}} \sum_{i=1}^{\text{H}} \sum_{t \in \mathcal{T}} \lambda_{g,t}(v_{g,t}^{(i)}) \Delta t.
\end{aligned} \tag{12}$$

Then, using Eq. (8), FR-2 under the quadratic NHPP model can be written as:

$$\begin{aligned}
\mathbb{E}[\Lambda_g(\mathbf{H}_g)] \;&=\; \lambda_{\text{norm}} T(1 - \alpha) \;+\; \lambda_{\text{norm}} \alpha \Delta t \frac{1}{\text{H}} \sum_{i=1}^{\text{H}} \sum_{t \in \mathcal{T}} f^2(v_{g,t}^{(i)}) \\
&=\; \lambda_{\text{norm}} T(1 - \alpha) \;+\; \lambda_{\text{norm}} \alpha \Delta t \sum_{t \in \mathcal{T}} \mathbb{E}[f^2(v_{g,t})].
\end{aligned} \tag{13}$$

FR-1 is computed using the ensemble-averaged velocities, and thus variability in the velocities across ensemble members is not accounted for. In contrast, FR-2 is obtained using the failure rate for each ensemble member; each failure rate is computed using the ensemble member-specific velocities as input. Thus FR-2 more properly incorporates uncertainty in the wind field, as represented by the variability in velocities across ensemble members. In this work, we compute both FR-1 and FR-2 for historical hurricanes, then compare the differences. The following result shows that FR-2 is greater than or equal to FR-1:

Proposition 2.1. *For a location g and wind velocities $\mathbf{H}_g$, the following holds for the failure rate Λ_g:*

$$\mathbb{E}[\Lambda_g(\mathbf{H}_g)] \;\geqslant\; \Lambda_g(\mathbb{E}[\mathbf{H}_g]) \tag{14}$$

The proof of Proposition 2.1 is provided in Appendix A, and requires a simple application of Jensen's inequality.

Next we define two estimates of the failure distribution in a location g, which incorporate FHLO. In defining the distribution estimates, we assume a very large (infinite) number of assets, in order to focus on the relationship

between wind velocities and the failure distributions rather than the effect of infrastructure-specific characteristics (i.e., number of assets).

Let $\Pr(s_g \mid x)$ refer to the Poisson distribution given by Eq. (2), which determines the number of failures s_g in location g under Poisson parameter x. Then, the distribution estimates are given as follows:

- **Failure Distribution A (FD-A)** is given by $\Pr(s_g \mid \mathbb{E}[\Lambda_g(\mathbf{H}_g)])$, i.e., the Poisson distribution with the ensemble-averaged failure rate (FR-2) as the distribution's Poisson parameter.

- **Failure Distribution B (FD-B)** is an ensemble-averaged distribution obtained as follows: First, for each ensemble member i, we obtain a Poisson distribution which uses $\Lambda_g^{(i)} = \Lambda_g(\tilde{\mathbf{H}}_g^{(i)})$ as the Poisson parameter. Then, the probability that there are s_g failures in grid g is given by:

$$\Pr(s_g) = \frac{1}{\mathrm{H}} \sum_{i=1}^{\mathrm{H}} \Pr(s_g \mid \Lambda_g^{(i)}) \tag{15}$$

i.e., we consider that the distribution given by parameter $\Lambda_g^{(i)}$ for ensemble member i occurs with probability $1/\mathrm{H}$. This is a valid probability distribution because the probability mass owing to each ensemble member is $1/\mathrm{H}$ and there are H ensemble members.

FD-A is computed using the ensemble-averaged failure rate (FR-2), and thus variability in the failure rates across ensemble members is not accounted for. In contrast, FD-B is obtained using the ensemble member-specific Poisson distributions, which are parameterized by the ensemble member-specific failure rates. Thus FR-2 more properly incorporates wind field uncertainty that is represented by the empirical distribution of ensemble failure rates.

3 ANALYSIS

In this section, we analyze how spatial variability in the hurricane wind field and forecast uncertainties given by FHLO affect the NHPP-estimated failure rates. First we quantify the spatial extent of damage, as measured by what we define as the "critical zone" (see Section 3.1), the geographical region in which failure rates exceed a defined threshold. Then we analyze how varying hurricane parameters such as intensity, size, and asymmetries affect the critical zone area and asset density-normalized failure rates (see Section 3.2). Finally, we assess how forecast uncertainty affects the probabilistic estimates of infrastructure damage, using wind field forecasts given by FHLO for

Hurricanes Hermine and Michael (see Section 3.3).

3.1 Hurricane Critical Zone

For this subsection, we consider a simple, stylized axisymmetric model in which the hurricane track deterministically moves in a straight line from a defined initial (genesis) point x_0^h to final (lysis) point x_f^h. The hurricane travels at a constant rate given by V_{tr}, the hurricane translation speed. For a time duration t after hurricane genesis, the track location is $x_t^h = x_0^h + V_{tr}t$. The parameters x_0^h, x_f^h, and V_{tr} are length-2 vectors, to separately model the hurricane's north-south and east-west movement.

Given the hurricane track, we estimate the wind field $\tilde{\mathbf{H}} = \{v_{g,t}\}_{g \in \mathcal{G}, t \in \mathcal{T}}$, which consists of velocities defined at grids $g \in \mathcal{G}$ and times $t \in \mathcal{T}$. Here, $\mathcal{T} = \{t_0, ..., t_f\}$, where hurricane genesis occurs at time t_0 in location x_0^h and dissipates at time t_f in location x_f^h. We assume that the wind field at a time t, defined as $\tilde{\mathbf{H}}_t = \{v_{g,t}\}_{g \in \mathcal{G}}$, is given by the parametric Holland model (Holland, 1980). In the Holland model, the velocity $v_{g,t}$ is a function of radial distance $r_{g,t}$ from the storm center:

$$v_{g,t}(r_{g,t}) = V_m \left(\frac{R_m}{r_{g,t}}\right)^{B/2} \exp\left(\frac{1}{2}\left(1 - \left(\frac{R_m}{r_{g,t}}\right)^B\right)\right), \tag{16}$$

where $r_{g,t} = \left\|x_g - x_t^h\right\|_2$ (L2 norm) and x_g denotes the centre-point of grid g. The Holland model has three wind field parameters, namely maximum intensity (V_m), radius of maximum winds (R_m), and shape parameter (B). The maximum intensity V_m is the maximum velocity in the surface wind field. The radius of maximum winds R_m is the radial distance at which the hurricane's velocity reaches V_m, and is a measure of hurricane size. The velocity increases with radius $r_{g,t}$ for $r_{g,t} < R_m$, and decreases with increasing $r_{g,t}$ for $r_{g,t} > R_m$. The shape parameter B governs the rate of decay of the wind velocities. Here, we assume that the Holland parameters remain constant for the duration of the storm and $B = 1$.[7]

Next, we define the so-called hurricane "critical zone", a measure of the spatial extent of hurricane-induced damage:

Definition 3.1. *Consider a hurricane wind field $\tilde{\mathbf{H}}_t$ at time t for which the maximum intensity $V_m(t) \geqslant V_{thres}$, where*

---

[7]Typically B is between 1 and 2.5.

V_{thres} is a defined threshold velocity. Then the **critical zone** of $\tilde{\mathbf{H}}_t$ consists of all spatial locations $g \in \mathcal{G}$ for which (1) radius $r_{g,t} < R_m(t)$; or (2) $r_{g,t} \geqslant R_m(t)$ and $v_{g,t} \geqslant V_{thres}$, where $R_m(t)$ is the radius of maximum winds at time t. Furthermore, the **critical zone** of the entire wind field $\tilde{\mathbf{H}}$ consists of the union of the critical zones for the time-specific wind fields $\tilde{\mathbf{H}}_t$, $\forall t \in \mathcal{T}$.

If a wind field $\tilde{\mathbf{H}}_t$ at time t is axisymmetric, then the wind velocity $v_{g,t}$ is only dependent on radial distance $r_{g,t}$ and we can define a so-called "critical radius":

Definition 3.2. *Assume that for an axisymmetric hurricane wind field $\tilde{\mathbf{H}}_t$ at time t, $V_m(t) \geqslant V_{thres}$. Then, the* ***critical radius*** *$R_{crit}(V_{thres}, t)$ is defined as a radius $r \geqslant R_m$ at which the velocity $v = V_{thres}$.*

Note that if the maximum intensity $V_m(t) < V_{thres}$ at time t, then the wind field $\tilde{\mathbf{H}}_t$ does not have a critical zone or critical radius.

According to Definitions 3.1-3.2, the **critical zone** of an axisymmetric wind field $\tilde{\mathbf{H}}_t$ consists of all spatial locations g for which the radius $r_{g,t}$ is less than the defined critical radius $R_{crit}(V_{thres}, t)$. We now present a simple result, under the restriction that we consider the simple, stylized axisymmetric hurricane model:

Lemma 3.3. *Assume that a hurricane has a straight-line track and constant translation speed V_{tr}. Furthermore, the hurricane has a Holland wind field given by Eq. (16) with constant Holland parameters, maximum intensity $V_m \geqslant V_{thres}$, and a defined critical radius $R_{crit}(V_{thres})$ (with a slight abuse of notation, V_m and R_{crit} are constant with time and thus not a function of t). Then, the critical zone of a hurricane wind field $\tilde{\mathbf{H}}$ forms an obround with area A_{crit} given by:*

$$A_{crit} = 2R_{crit}(V_{thres})T\|V_{tr}\|_2 + \pi[R_{crit}(V_{thres})]^2, \tag{17}$$

where T is the hurricane lifetime, the obround's rectangle length $T\|V_{tr}\|_2$ is the distance covered by the hurricane track, and the rectangle width is given by two times the critical radius $R_{crit}(V_{thres})$. The first half-circle at one end of the obround corresponds to one-half of the critical zone area for the hurricane at genesis. The second half-circle at the other end corresponds to one-half of the critical zone area for the hurricane at lysis.

For the remainder of the paper, we will focus on the quadratic NHPP model and set $V_{thres} = V_{crit}$, where V_{crit} is the model's critical velocity parameter. This case is particularly important, because the Poisson intensity is equal to λ_{norm} when the hurricane velocity is below V_{crit}. Under this specific model, we present a further result:

Proposition 3.4. *For the quadratic NHPP model given by Eq. (5) and the parameter* $V_{\text{thres}} = V_{\text{crit}}$, *the failure rate* $\Lambda_g > \lambda_{norm} T$ *if and only if a spatial location g falls in the critical zone of an axisymmetric hurricane* $\tilde{\mathbf{H}}$ *with duration* T.

Proof. If location g is not in the critical zone of $\tilde{\mathbf{H}}$, then the Poisson intensity $\lambda_{g,t} = \lambda_{\text{norm}}$ at all times $t \in \mathcal{T}$ and thus $\Lambda_g = \lambda_{\text{norm}} T$. If g is in the critical zone of $\tilde{\mathbf{H}}$, then the velocity $v_{g,t} > V_{\text{crit}}$ for at least one time $t \in \mathcal{T}$ (following Definitions 3.1-3.2). Since velocity $v_{g,t}$ exceeds V_{crit}, we have $\lambda_{g,t} > \lambda_{\text{norm}}$ and from Eq. (8), we conclude that $\Lambda_g > \lambda_{\text{norm}} T$. □

The results given by Lemma 3.3 and Proposition 3.4 will be relevant in the next subsection, where we compute the critical zone area and failure rates under the simple, stylized axisymmetric model we consider here.

3.2   Analyzing Spatial Variability of Damage

In this subsection, we discuss how the critical zone area and spatial variability of estimated failure rates are dependent on the hurricane parameters of maximum intensity V_m and radius of maximum winds R_m. Then we discuss how introducing asymmetries (Uhlhorn et al., 2014; Chang, Amin, & Emanuel, 2020), or variabilities in wind velocity with respect to the azimuthal angle[8], would alter the critical zone and failure rates.

Figure 3 (resp. Figure 4) illustrates the dependency of the critical zone and failure rates on maximum intensity V_m (resp. radius of maximum winds R_m), for an axisymmetric wind field. Figure 5 demonstrates how the critical zone and failure rates vary with V_m, when we introduce an asymmetry by adding the storm-translation vector to the Holland wind field.[9] In this case, the maximum velocity under equal radius occurs at exactly $90°$ clockwise of the translation direction, where the storm motion and cyclostrophic wind direction are aligned. This is reflected in Figure 5, where the storm is translating northward, the maximum failure rates occur in a wall east of the storm track, and the critical zones no longer display the obround shapes suggested by Eq. (17).

Tables 1-3 respectively list the critical zone area A_{crit}, maximum failure rate, and average failure rate within the critical zone under varying values of V_m and R_m, for hurricane wind fields with or without asymmetries. Furthermore, in Appendix B, we formulate parametric models that relate the Holland parameters to critical radius and

---

[8]Azimuthal angle is measured as degrees clockwise from a defined reference direction (typically the storm translation direction)

[9]Storm translation and wind shear are considered important environmental variables in determining the physical structure of a storm's asymmetries. Asymmetries can also be accounted for by setting a Holland parameter, such as V_m, to be a function of these environmental inputs (Chang, Amin, & Emanuel, 2020).

critical zone area. Both the critical zone area and maximum failure rate achieved increase with V_m and R_m, but the rate of increase is faster with respect to V_m. The maximum failure rate is also higher under asymmetric hurricanes, due to the high wind velocities occurring east of the storm track, as shown in Figure 5. In addition, the discrepancy in maximum failure rate between the axisymmetric and asymmetric hurricanes increases with V_m. This suggests that not accounting for asymmetries in hurricane wind field forecasts can lead to significant underestimation of failure rates due to high-intensity hurricanes. In addition, the average failure rate in the critical zone is greater when asymmetry is included.

Once the conditions of straight-line hurricane track and time-constant Holland wind field parameters are relaxed, the critical zone area and variability in failure rates would differ from what is suggested in Figures 3-5. For instance, hurricane maximum intensity V_m is time-varying, and usually lower at the beginning and end of the hurricane's lifetime. Furthermore, the Holland wind field considered here only includes one shape parameter, but additional shape parameters would affect the decay in wind velocities with radial distance; the updated Holland 2010 model (Holland, Belanger, & Fritz, 2010) includes more shape parameters.

3.3   Analyzing Effect of Forecast Uncertainty on Damage

Now, we assess how forecast uncertainty given by FHLO affects the NHPP-estimated failure rates and failure distributions.[10] Our analysis focuses on 1,000-member ensemble simulations for Hurricanes Hermine (2016) and Michael (2018); parameters used for the simulations given by FHLO are listed in Table 4. Hermine is a Category 1 hurricane, whereas Michael is a highly intense, Category 5 hurricane that reached peak maximum intensities of around 70 m/s. Both hurricanes made landfall in northwestern Florida.

Analysis for Hurricane Hermine: Figure 6 plots Hermine's wind field $\tilde{\mathbf{H}}$ and corresponding Poisson intensities $\lambda_{g,t}$ at six designated times t, for a single ensemble member. Figure 7 plots Hurricane Hermine's ensemble-averaged wind field $\mathbb{E}[\mathbf{H}] = \{\bar{v}_{g,t}\}_{g \in \mathcal{G}, t \in \mathcal{T}}$. The velocity contours are much smoother after averaging, and the majority of the geographical region does not contain significant velocity exceedances above the critical velocity parameter V_{crit}. More specifically, critical velocity exceedances within $\mathbb{E}[\mathbf{H}]$ occur for only six out of the 121 times for which the wind field forecast is available.

---

[10]For computation of failure rates (FR-1 and FR-2), we obtain the asset density-normalized failure rate for each grid, then multiple it by the asset density. We considered The City of Tallahassee Utilities, which has 1,800 km of distribution lines over 255 km^2, averaging to 7.08 km of line/km^2 area (Myers & Yang, July 15, 2020). Furthermore, we assume each location g has an area of 1 km^2.

Figure 8 demonstrates how spatially-varying failure rates differ depending on the choice of FR-1 vs. FR-2. Recall that in Section 2.3, we proved FR-2 is greater than or equal to FR-1. When using FR-1 as the failure rate estimate, only 20.9% of the considered geographical region (4,414 km^2) falls within the critical zone. In contrast, 100% of the considered geographical region falls within the critical zone when using FR-2. Furthermore, the region-averaged failure rate is 0.12 failures/kilometer of assets for FR-1 and 3.34 for FR-2. This suggests that failure rates are, on average, more than 28 times higher under FR-2. The main reason for this discrepancy is that supercritical velocities (wind velocities greater than the defined critical threshold V_{crit}) are averaged out if FR-1 is used, whereas FR-2 considers the individual ensemble member wind fields in failure rate estimation. In this sense, FR-2 is more realistic, as the supercritical velocities in the ensemble member wind fields are accounted for in failure rate estimation.

Figure 9 demonstrates how the probability distribution over the number of failures depends on the choice of FD-A vs. FD-B. The spatial locations associated with the distributions in Figure 9 differ in terms of minimum radial distance to the storm center achieved during the hurricane's lifetime. Both distributions are right-skewed, but FD-B is especially so: the probability given by FD-B is maximum at zero failures and decreases with increasing number of failures. Furthermore, FD-B has a more pronounced tail than FD-A. Amongst the four locations, it is anywhere between 4.6 and 80 times more likely to have nine or more failures when using FD-B in place of FD-A. The difference in the probability of 9+ failures, as given by FD-A vs. FD-B, is greater for locations that are farther from the storm track. This suggests that FD-A particularly underestimates the probabilities of high-damage outcomes for locations in the storm periphery.

Analysis for Hurricane Michael: Figure 10-12 demonstrate how the failure rates given by FR-1 and FR-2 differ for Michael. Due to Michael's high intensity, its ensemble-averaged wind field contains more frequent and significant exceedances of the critical velocity (occurring at 26 out of the 121 times) in comparison to Hermine (see Figure 11). As a result, estimates of FR-1 are also much higher (see Figure 12). The region-averaged failure rate is 2.69 failures/kilometer of assets for FR-1 and 4.48 for FR-2, which implies that the average failure rate is 1.67 times higher under FR-2. The difference between FR-1 and FR-2 is less pronounced than for Hermine, because Michael is a high-intensity hurricane and hence a more significant portion of the geographical region falls in the critical zone under FR-1.

Figure 13 demonstrates how the failure distributions given by FD-A and FD-B differ for Michael. As a result of

Michael's high intensity, the probability distributions have more pronounced tails and less right-skewedness than under Hermine.

4   PREDICTING OUTAGES IN HISTORICAL HURRICANES

A lack of accurate damage predictions can impede estimates of loss-of-service within infrastructure systems. Improved estimation of loss-of-service is desirable in estimating hurricane-induced risk on the infrastructure system, as well as in informing proactive strategies to maintain post-disaster infrastructural functionality. In Section 3, we focused on the spatial variability in NHPP estimates of probabilistic damage and effects of forecast uncertainty given by FHLO. In this section, we consider the relationship between damage and loss-of-service. Specifically, we analyze the accuracy of estimated NHPP failure rates in predicting loss-of-service within electric power infrastructure resulting from Hurricane Michael. For electricity networks, we consider that loss-of-service is given by outages, or loss of electrical power network supply to customers. The failure rates (FR-2) are estimated using wind field forecasts given by FHLO as input (see Section 2.3).

We discuss the computational setup in Section 4.1: the application of FHLO and NHPP, the selected geographical region of interest, and the outage data employed. Our analysis focuses on the northwestern Florida region (including the Tallahassee urban area), where Hurricane Michael made landfall. In Section 4.2, we formulate regression models to predict outages, and demonstrate that a statistically significant relationship exists between the estimated failure rates and outage rates. In Section 4.3, we discuss insights obtained from studying the estimated regression models.

4.1   Computational Setup

The probabilistic wind field forecast for Michael is given by a 1,000-member ensemble forecast using FHLO. For each ensemble member, the velocity is forecasted at locations within the latitude range $29.3°$N to $32.2°$N and longitude range $82.6°$W to $88.7°$W, with $0.1° \times 0.1°$ grid spacing. The forecast is initialized on October 9, 2018 at 12Z (Coordinated Universal Time). This time corresponds with around 8:00am Eastern Daylight Time (EDT), which is about 1.5 days before Michael made landfall near Mexico Beach, Florida.

We obtain outage data from the Florida Division of Emergency Management (Ray & Yang, July 23, 2020). Our analysis focuses on October 10-12, the days during and immediately after Michael's landfall in Florida. On these

three days, outage data is available at six different times given in Eastern Daylight Time (EDT): October 10, 15:40; October 10, 16:35; October 10, 19:50; October 11, 19:40; October 11, 22:00; and October 12, 23:05. At each time, the outages are measured by number of households without power in each county. The total number of households and geographical area associated with each county are also included in the data. Using this data, one can compute the total number of outages per county, the percentage of households experiencing outages, as well as percentage or number of households with outages normalized by area. We focus on outages in the counties of Northern Florida (particularly the Tallahassee area).

To compare outages to failure rates (FR-2), we first estimate the failure rates in each county on an hourly basis using the quadratic NHPP model (Section 2.2). This requires computing the Poisson intensity $\lambda_{g,t}^{(i)}$ using Eq. (5) in each $0.1° \times 0.1°$ grid g, at each hour t, and for each ensemble member i. For a grid g, the ensemble-averaged failure rate $\Lambda_g(t')$ at a given time $t' \leqslant t_{\mathrm{f}}$ (where t_{f} corresponds to Oct. 14 at 12Z, the last time for which FHLO is available) is given by:

$$\Lambda_g(t') \;=\; \frac{1}{\mathrm{H}} \sum_{i=1}^{\mathrm{H}} \sum_{t=t_0}^{t'} \lambda_{g,t}^{(i)}. \tag{18}$$

This summation is similar to Eq. (1), except that the summation is taken over $t \in \{t_0, ..., t'\}$ rather than $t \in \mathcal{T}$ where $\mathcal{T} = \{t_0, ..., t_{\mathrm{f}}\}$. These failure rates are expected to be increasing with time t', reflecting accumulated exposure of the electric power infrastructure to hurricane winds over time. Then, we map the grid-wise failure rates to county-wise failure rates. To do so, we assign a grid to a county, if the majority of the grid's spatial area is occupied by said county. We obtain the county-wise failure rate by averaging the grid-wise failure rates corresponding to the county.

We also define the ensemble-averaged "cumulative velocity" at a time t' and for grid g as follows:

$$\mathcal{V}_g(t') \;=\; \frac{1}{\mathrm{H}} \sum_{i=1}^{\mathrm{H}} \sum_{t=t_0}^{t'} v_{g,t}^{(i)}, \tag{19}$$

i.e., it is the ensemble-averaged sum of the grid-specific velocities over all measurement times from t_0 to t'. Next we compute county-wise cumulative velocities, using the same procedure that we applied to the failure rates. The county-wise failure rates and cumulative velocities are used as inputs to regression models that predict outage rates.

In Figure 14, we plot the outage rates (number of outages per 100 households) and asset density-normalized failure rates (FR-2) in Northern Florida at four different times. Failure rates are calculated using Eq. (18). Figure 14a plots the outages and failure rates about three hours after Hurricane Michael made landfall in Florida. In contrast,

Figure 14d shows the results nearly 33 hours after landfall. The counties with high outages rates mostly fall in the critical zone of the hurricane, which corresponds to the counties where the failure rates are higher (denoted by light blue, green, orange or yellow colors), as opposed to sub-critical regions corresponding to dark blue. In particular, the highest outage and failure rates mostly occur in the geographical region between Panama City and Tallahassee.

4.2 Outage Rate Prediction via Regression Models

We estimate regression models that relate outage rate (outages per 100 households) to one of two inputs: failure rate (FR-2, Eq. (18)) or cumulative velocity (Eq. (19)). The cumulative velocity is employed in order to analyze the extent to which the critical velocity V_{crit} affects the outage prediction. According to the quadratic model, Poisson intensities are small and constant for velocities below V_{crit}. Thus we hypothesize that failure rates remain insignificant below a certain cumulative velocity threshold, which translates to near-zero outage rates. Our goal is to evaluate this hypothesis using the empirical observations of outages.

To assess the strength of cumulative velocities and failure rates as predictors of outage rates, we estimate binomial regression models (BRMs). In particular, the BRM gives the probability over number of successes out of a set of Bernoulli trials. In our case, a "success" is an outage and the number of "trials" is given by the number of households in a given county. We estimate a BRM for each input (cumulative velocity or failure rate) and at each time for which outage data is available. Figure 15 (resp. 16) plots the outage rate vs. cumulative velocity (resp. failure rate) at four different times; estimated binomial regression models are included in the plots. We find that cumulative velocity is a statistically significant predictor (p-value less than 0.05) at all considered times except October 12, 23:05 (about 58 hours after landfall), and failure rate is a statistically significant predictor at all times. For more details regarding implementation of the BRM, please see Appendix C.

4.3 Discussion

We observe from Figure 15 that the relationship between outage rate and cumulative velocity could be approximately represented by an S-shaped curve. The outage rate is near-zero and roughly constant for cumulative velocities below a certain threshold, which is consistent with inclusion of the critical velocity parameter in the NHPP model. Once this threshold is passed, we observe a rapid increase in the outage rate with cumulative velocity, because of

the quadratic relationship between Poisson intensity and velocity above V_{crit}. Then once the cumulative velocity becomes sufficiently high, the outage rate approaches 100%, i.e., saturation has occurred (see Eq. (3) in Section 2.2). In summary, the binomial regression model is able to account for the impact of the critical velocity as well as saturation on the outage rates.

Figures 14c-14d, which correspond to October 11, illustrate the effect of saturation. Specifically, a few counties (mostly between Panama City and Tallahassee) have outage rates of around 100% but noticeably differing failure rates. The variability in failure rates within this region may also result due to the network topology of distribution feeders in the power infrastructure, which is subject to physical laws and managed by system operators. For example, if a substation within a distribution feeder is disrupted, then power supply to all downstream loads will be interrupted. As another example, failure of a critical asset in the power infrastructure can cause multiple outages, whereas failure of non-critical assets may not cause any outage if the network is able to survive in the presence of these failures.

The cumulative velocity-outage rate relationship is not statistically significant on October 12, 23:05, because it has been over two days since Hurricane Michael made landfall in Northern Florida. Over the course of this time, Michael traveled northward; there was ample time for utilities to repair damage and restore electricity service. This suggests that cumulative velocity alone would not be a sufficient predictor of outages at this time, because spatially-varying repair rates become increasingly important with time.

5   ESTIMATING TOTAL DAMAGE AND FINANCIAL LOSSES

Finally, we estimate parametric models that relate total hurricane-induced damage and financial losses in an infrastructure system to two key storm parameters: intensity parameter V_m and size parameter R_m (see Section 3.1). The parametric models are estimated using the quadratic nonhomogeneous Poisson process (NHPP) model detailed in Section 2.2, to demonstrate simple power law relationships between damage, financial losses, and hurricane parameters (see Figure 17). Here, we assume that hurricanes have the same characteristics as were defined in Section 3.1.[11]

Parametric Function for Total Damage: While we can formulate an analytical solution for total damage Λ_{total}

---

[11]We do not employ FHLO in this section; incorporation of FHLO would require us to obtain wind field ensembles from a large number of historical hurricanes. The computational expense of calculating failure rates from all the ensembles would be high. Furthermore, hurricane intensity and size will vary temporally in FHLO, which would make estimating the parametric functions less straightforward. However it is also possible to repeat the exercise conducted in this section using FHLO.

(see Appendix D.1), it is not convenient to relate the analytical solution to V_m and R_m, due to the highly nonlinear nature of the Holland model. Consequently, we formulate a parametric function for Λ_{total} which accounts for the critical velocity parameter V_{crit} and the critical zone area A_{crit} (see Appendix D.2). With regards to V_{crit}, we consider the following function of V_m as an input to the parametric models:

$$g(V_m) = \frac{\max(V_{crit}, V_m) - V_{crit}}{V_{crit}} \tag{20}$$

The function $g(V_m) = 0$ if $V_m \leqslant V_{crit}$, and increases linearly with V_m otherwise.

Based on the estimated model parameters, Λ_{total} is roughly proportional to R_m^2 and $[g(V_m)]^{2.26}$ when $V_m \geqslant V_{crit}$, as opposed to the quadratic relationship between location-specific failure rate and velocity in Eq. (5). This power law relationship can be expressed as:

$$\Lambda_{total}(V_m, R_m) \sim O\big(R_m^2(V_m - V_{crit})^{2.3}\big). \tag{21}$$

Parametric Function for Total Financial Loss: For the purpose of financial loss modeling, we formulate a network repair model that ensures the financial loss associated with a given location scales quadratically with the number of local failures (see Appendix E.1). As is the case for total damage, the analytical solution for total financial loss (see Appendix E.2) cannot conveniently incorporate V_m and R_m as inputs. Instead, we formulate a parametric model for total financial loss L_{total} that considers the power law relationship for damage suggested by Eq. (21) and the network repair model in Appendix E.1. Based on the estimated model parameters, L_{total} is roughly proportional to R_m^3 and $[g(V_m)]^{5.6}$ when $V_m \geqslant V_{crit}$. Because of the quadratic relationship between location-specific financial loss and number of damages, the polynomial orders associated with R_m and $g(V_m)$ for L_{total} are expectedly greater than those for expected damage Λ_{total}. The associated power law relationship can be expressed as (see Appendix E.3):

$$L_{total}(V_m, R_m) \sim O\big(R_m^3(V_m - V_{crit})^{5.6}\big). \tag{22}$$

For Eq. (21)-(22), we do not account for finiteness in the total number of assets. However, in Appendix D.3, we discuss how computed total damage would differ when saturation is incorporated in the damage estimation.

Previous work (Nordhaus, 2006) has suggested that total hurricane-induced financial losses are roughly a function of V_m to the 8-th power. In contrast, we estimate the relationship between total financial losses and $g(V_m)$, rather than V_m. This accounts for our expectation of insignificant damage below the critical velocity V_{crit}, which we

showed is in agreement with empirical observations in Section 4. By using $g(V_m)$ as a predictor, we estimate that total losses are roughly proportional to $V_m - V_{crit}$ to the 5.6-th power, when $V_m \geqslant V_{crit}$. In contrast, when we used V_m as a predictor, we found that losses were proportional to V_m to the 7.8-th power.

6 CONCLUDING REMARKS

In this paper, we introduce a modeling approach for probabilistic estimation of hurricane wind-induced damage to infrastructural assets. Our approach uses a Nonhomogeneous Poisson Process (NHPP) model to estimate spatially-varying probability distributions of damage as a function of the hurricane wind velocities. The NHPP model is applied to failures of overhead assets in electricity distribution systems, and features a quadratic relationship between the Poisson intensity and wind velocity above a critical velocity threshold. In order to incorporate hurricane forecast uncertainty in estimation of the distributions, we employ Forecasts of Hurricanes using Large-Ensemble Outputs (FHLO) as inputs into the NHPP model.

The NHPP model's critical velocity parameter motivates us to define the "critical zone", a measure of the spatial extent of hurricane-induced damage. Using a simple model of the hurricane that incorporates the axisymmetric Holland wind field, we demonstrate how the critical zone and failure rates are dependent on hurricane intensity, size, and asymmetries. Then we show that not incorporating forecast uncertainty given by FHLO results in underestimation of failure rates, and assess the degree of underestimation under two hurricanes of different intensities (Hermine and Michael). In addition, we empirically demonstrate that improperly estimating probability distributions of damage results in underestimation of high-damage scenarios. These findings suggest that forecast uncertainty plays a critical role in estimation of hurricane-induced damage.

Our modeling approach is able to accurately predict outages resulting from Hurricane Michael. By fitting binomial regression models (BRMs), we demonstrate that failure rate and cumulative velocity are statistically significant predictors of the outage rate. The fitted BRMs also demonstrate that empirical observations are reflective of the critical velocity parameter in the NHPP model, and that the outage rates saturate at 100% once failure rates are sufficiently high. Finally, we fit simple parametric models that relate total damage and financial losses to key hurricane parameters (intensity and size). Under a simple, stylized hurricane model, we show that total damage is proportional to intensity (resp. size) to the 2.3-th (resp. 2-th) power, and that total financial losses is proportional to intensity

(resp. size) to the 5.6-th (resp. 3-rd) power.

Future work on this topic will focus on the joint effects of damage and network topology on infrastructure system loss-of-service. Network topology determines connectivity between the service producers and end-users, as well as the criticality of various infrastructure assets, such that damage of more critical assets results in an especially significant loss-of-service. It is also worth noting that this work focuses on hurricane winds, rather than other relevant physically-based threats induced by hurricanes. These threats, such as storm surge and rainfall, can also cause substantial damage to infrastructure systems.

A second avenue of future work is to apply improved damage and loss-of-service estimates to the design of proactive (pre-storm) strategies that minimize hurricane wind-induced risk on infrastructure systems. Accurate estimation of spatially-varying damage minimizes risk by not only improving the optimality of proactive strategies, but also by increasing the efficiency of damage localization and repair. For instance, a plethora of works address optimal proactive allocation of distributed energy resources (DERs) (Gao, Chen, Mei, Huang, & Xu, 2017; Sedzro, Lamadrid, & Zuluaga, 2018; Chang, Shelar, & Amin, 2018, 2020) in distribution feeders of electric power infrastructure; our work is readily applicable to the proposed methods in these works. Indeed, research demonstrates that energy customers are willing to pay for back-up electricity services during large outages of long duration (Baik, Davis, Park, Sirinterlikci, & Morgan, 2020).

REFERENCES

Alvehag, K., & Söder, L. (2011). A Reliability Model for Distribution Systems Incorporating Seasonal Variations in Severe Weather. *IEEE Transactions on Power Delivery*, *26*(2), 910–919.

Baik, S., Davis, A. L., Park, J. W., Sirinterlikci, S., & Morgan, M. G. (2020). Estimating what US residential customers are willing to pay for resilience to large electricity outages of long duration. *Nature Energy*, *5*(3), 250–258.

Brown, R., Gupta, S., Christie, R., Venkata, S., & Fletcher, R. (1997). Distribution System Reliability Assessment: Momentary Interruptions and Storms. *IEEE Transactions on Power Delivery*, *12*(4), 1569–1575.

Campbell, R. (2013, 01). Weather-related Power Outages and Electric System Resiliency. , 103-118.

Center, N. H. (n.d.). *Definition of the NHC Track Forecast Cone.* `https://www.nhc.noaa.gov/aboutcone.shtml`.

Chang, D., Amin, S., & Emanuel, K. (2020). Modeling and Parameter Estimation of Hurricane Wind Fields with Asymmetry. *Journal of Applied Meteorology and Climatology*, *59*(4), 687–705.

Chang, D., Shelar, D., & Amin, S. (2018). DER Allocation and Line Repair Scheduling for Storm-induced Failures in Distribution Networks. In *2018 IEEE SmartGridComm* (pp. 1–7).

Chang, D., Shelar, D., & Amin, S. (2020). Stochastic Resource Allocation for Electricity Distribution Network Resilience. In *2020 American Control Conference* (pp. 1–6).

Chavas, D. R., Lin, N., & Emanuel, K. (2015). A Model for the Complete Radial Structure of the Tropical Cyclone Wind Field. Part I: Comparison with Observed Structure. *J ATMOS SCI*, *72*(9), 3647–3662.

Emanuel, K. (2004). Tropical Cyclone Energetics and Structure. *Atmospheric Turbulence and Mesoscale Meteorology*, *8*, 165–191.

Emanuel, K. (2005). Increasing destructiveness of tropical cyclones over the past 30 years. *Nature*, *436*(7051), 686.

Emanuel, K. (2011). Global warming effects on u.s. hurricane damage. *Weather, Climate, and Society*, *3*(4), 261–268.

Emanuel, K. (2017). A fast intensity simulator for tropical cyclone risk analysis. *Natural Hazards*, *88*(2), 779–796.

Emanuel, K., DesAutels, C., Holloway, C., & Korty, R. (2004). Environmental Control of Tropical Cyclone Intensity. *Journal of the Atmospheric Sciences*, *61*(7), 843–858.

Gao, H., Chen, Y., Mei, S., Huang, S., & Xu, Y. (2017, July). Resilience-Oriented Pre-Hurricane Resource Allocation in Distribution Systems Considering Electric Buses. *Proceedings of the IEEE*(7). doi: 10.1109/JPROC.2017.2666548

Hamill, T. M., Whitaker, J. S., Fiorino, M., & Benjamin, S. G. (2011). Global Ensemble Predictions of 2009's Tropical Cyclones Initialized with an Ensemble Kalman Filter. *Monthly Weather Review*, *139*(2), 668–688.

Han, S.-R., Guikema, S. D., Quiring, S. M., Lee, K.-H., Rosowsky, D., & Davidson, R. A. (2009). Estimating the spatial distribution of power outages during hurricanes in the Gulf coast region. *Reliability Engineering & System Safety*, *94*(2), 199–210.

Holland, G. J. (1980). An Analytic Model of the Wind and Pressure Profiles in Hurricanes. *Monthly Weather Review*, *108*(8), 1212-1218. Retrieved from `https://doi.org/10.1175/1520-0493(1980)108<1212:` `AAMOTW>2.0.CO;2` doi: 10.1175/1520-0493(1980)108<1212:AAMOTW>2.0.CO;2

Holland, G. J., Belanger, J. I., & Fritz, A. (2010). A Revised Model for Radial Profiles of Hurricane Winds. *Monthly Weather Review*, *138*(12), 4393–4401.

Lallemand, C. (2008). Methodology for a risk based asset management. *Royal Institute of Technology*.

Lee, A. C., Dahan, M., Weinert, A. J., & Amin, S. (2019). Leveraging sUAS for Infrastructure Network Exploration and Failure Isolation. *Journal of Intelligent & Robotic Systems*, *93*(1-2), 385–413.

Li, G., Zhang, P., Luh, P. B., Li, W., Bie, Z., Serna, C., & Zhao, Z. (2014). Risk Analysis for Distribution Systems in the Northeast US under Wind Storms. *IEEE Trans. Power Syst.*, *29*(2), 889–898.

Lin, J., Emanuel, K., & Vigh, J. L. (2020). Forecasts of Hurricanes using Large-Ensemble Outputs. *Weather and Forecasting*, *35*(5), 1713–1731.

Liu, H., Davidson, R. A., & Apanasovich, T. V. (2007, Nov). Statistical Forecasting of Electric Power Restoration Times in Hurricanes and Ice Storms. *IEEE Transactions on Power Systems*, *22*(4), 2270-2279. doi: 10.1109/TPWRS.2007.907587

Liu, H., Davidson, R. A., Rosowsky, D. V., & Stedinger, J. R. (2005). Negative Binomial Regression of Electric Power Outages in Hurricanes. *Journal of Infrastructure Systems*, *11*(4), 258–267.

Majumdar, S. J., & Finocchio, P. M. (2010). On the Ability of Global Ensemble Prediction Systems to Predict Tropical Cyclone Track Probabilities. *Weather and Forecasting*, *25*(2), 659–680.

Myers, S., & Yang, V. (July 15, 2020). Email Communication. 300 S. Adams St., Tallahassee, FL 32301.

Nordhaus, W. D. (2006). *The Economics of Hurricanes in the United States* (Tech. Rep.). National Bureau of Economic Research.

Patricola, C. M., & Wehner, M. F. (2018). Anthropogenic influences on major tropical cyclone events. *Nature*, *563*(7731), 339–346.

Ray, J., & Yang, V. (July 23, 2020). Email Communication. 2555 Shumard Oak Blvd, Tallahassee, FL 32399.

Sedzro, K. S. A., Lamadrid, A. J., & Zuluaga, L. F. (2018, May). Allocation of Resources Using a Microgrid Formation Approach for Resilient Electric Grids. *IEEE Transactions on Power Systems*, *33*(3), 2633-2643. doi: 10.1109/TPWRS.2017.2746622

Stocks, K., & Yang, V. (July 29, 2020). Email Communication. 6724 Thomasville Rd, Tallahassee, FL 32312.

Uhlhorn, E. W., Klotz, B. W., Vukicevic, T., Reasor, P. D., & Rogers, R. F. (2014). Observed Hurricane Wind Speed Asymmetries and Relationships to Motion and Environmental Shear. *Monthly Weather Review*, *142*(3), 1290–1311.

Van Hentenryck, P., Bent, R., & Coffrin, C. (2010). Strategic Planning for Disaster Recovery with Stochastic Last Mile Distribution. In *CPAIOR* (pp. 318–333).

Vickery, P. J., Skerlj, P., Steckley, A., & Twisdale, L. (2000). Hurricane Wind Field Model for Use in Hurricane Simulations. *Journal of Structural Engineering*, *126*(10), 1203–1221.

Vickery, P. J., Wadhera, D., Powell, M. D., & Chen, Y. (2009). A Hurricane Boundary Layer and Wind Field Model for Use in Engineering Applications. *Journal of Applied Meteorology and Climatology*, *48*(2), 381–405.

Xie, L., Bao, S., Pietrafesa, L. J., Foley, K., & Fuentes, M. (2006). A Real-Time Hurricane Surface Wind Forecasting Model: Formulation and Verification. *Monthly Weather Review*, *134*(5), 1355–1370.

Zhou, Y., Pahwa, A., & Yang, S.-S. (2006). Modeling Weather-related Failures of Overhead Distribution Lines. *IEEE Trans. Power Syst..*

Tables

		Radius of maximum winds (R_m)					
		20 km		30 km		40 km	
Intensity (V_m)		Axi	Asym	Axi	Asym	Axi	Asym
Tropical Storm	25 m/s	1.36×10^5	1.49×10^5	2.10×10^5	2.30×10^5	2.86×10^5	3.14×10^5
Category 1	37 m/s	4.02×10^5	4.35×10^5	6.09×10^5	6.59×10^5	8.15×10^5	7.77×10^5
Category 2	46 m/s	6.61×10^5	7.11×10^5	9.75×10^5	8.49×10^5	12.82×10^5	9.70×10^5

Table 1: Critical zone area A_{crit} (km^2) associated with hurricanes under varying intensity V_m and radius of maximum winds R_m. "Axi" refers to an axisymmetric wind field, and "Asym" refers to an asymmetric wind field with asymmetry owing to the storm translation vector.

		Radius of maximum winds (R_m)					
		20 km		30 km		40 km	
Intensity (V_m)		Axi	Asym	Axi	Asym	Axi	Asym
Tropical Storm	25 m/s	0.4	0.8	0.6	1.2	0.9	1.5
Category 1	37 m/s	3.8	4.5	5.7	6.7	7.6	9.0
Category 2	46 m/s	8.6	9.6	12.9	14.4	17.2	19.1

Table 2: As in Table 1, but for the maximum failure rate (failures/km) achieved in the critical zone. Here, the threshold failure rate for a location g to belong in the critical zone is given by $\lambda_{norm} T = 0.0042$ failures/km (following Proposition 3.4).

		Radius of maximum winds (R_m)					
		20 km		30 km		40 km	
Intensity (V_m)		Axi	Asym	Axi	Asym	Axi	Asym
Tropical Storm	25 m/s	0.2	0.3	0.3	0.5	0.5	0.6
Category 1	37 m/s	1.5	1.6	2.2	2.3	2.9	3.4
Category 2	46 m/s	2.9	3.0	4.3	5.4	7.3	7.6

Table 3: As in Table 2, but for the average failure rate (failures/km) achieved in the critical zone.

	Hermine	Michael
Latitude range North-south length	29.70°N $- 30.69^\circ$N 110 km	29.60°N $- 32.20^\circ$N 289 km
Longitude range East-west length	83.21°W $- 85.20^\circ$W 192 km	83.40°W $- 86.50^\circ$W 300 km
Initialization time	September 1, 2016 at 0z	October 9, 2018 at 12Z

Table 4: Parameter choices for simulations given by Forecasts of Hurricanes using large-Ensemble Outputs (FHLO) for Hurricanes Hermine and Michael. We assume $0.1^\circ \times 0.1^\circ$ grids within the considered latitude and longitude range. Simulated wind velocities are given at 121 times t spaced one hour apart from each other, starting from the initialization time given in Coordinated Universal Time.

Figures
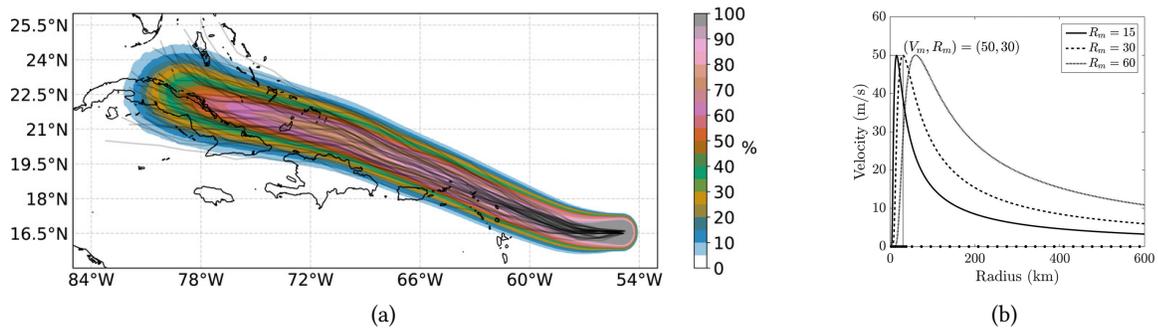
Figure 1: (a) – Example of a track simulation for Hurricane Irma from Forecasts of Hurricanes using Large-Ensemble Outputs, adapted from Lin, Emanuel, & Vigh, 2020. (b) – Illustration of how hurricane velocity varies with radius from the storm center using the parametric Holland 1980 model. The winds are low (near zero) at the hurricane eye, increase rapidly with radius and peak at the hurricane eye wall, then decrease with increasing radius outside the eye wall.
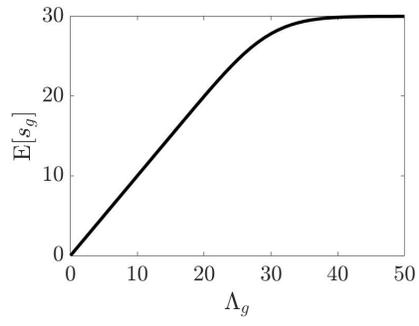
Figure 2: Expected number of failures $\mathbb{E}[s_g]$ given by Eq. (4) vs. failure rate Λ_g.
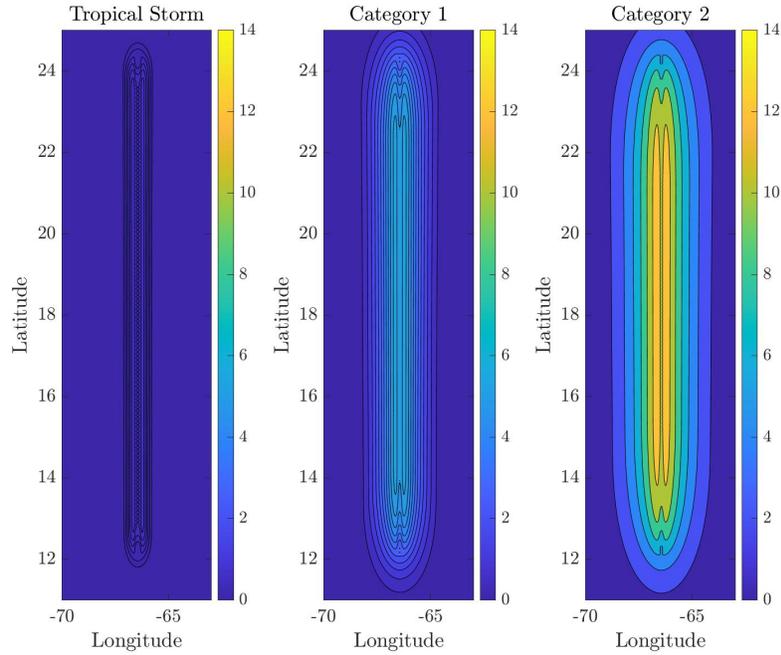
Figure 3: Spatially-varying failure rates as a function of a hurricane wind field, under different maximum intensities V_m. An axisymmetric Holland wind field with time-constant Holland parameters is used (see Section 3.1). Parameters are: $V_{tr} \approx 3$ m s^{-1}, $R_m = 30$ km, $B = 1$. The choices of V_m are 25 m s^{-1} (*left*), 37 m s^{-1} (*center*), and 46 m s^{-1} (*right*), corresponding respectively to tropical storm, Category I, and Category II on the Saffir-Simpson scale. The obround in each subfigure indicates the critical zone, and failure rates are given as failures per kilometer of infrastructure assets.
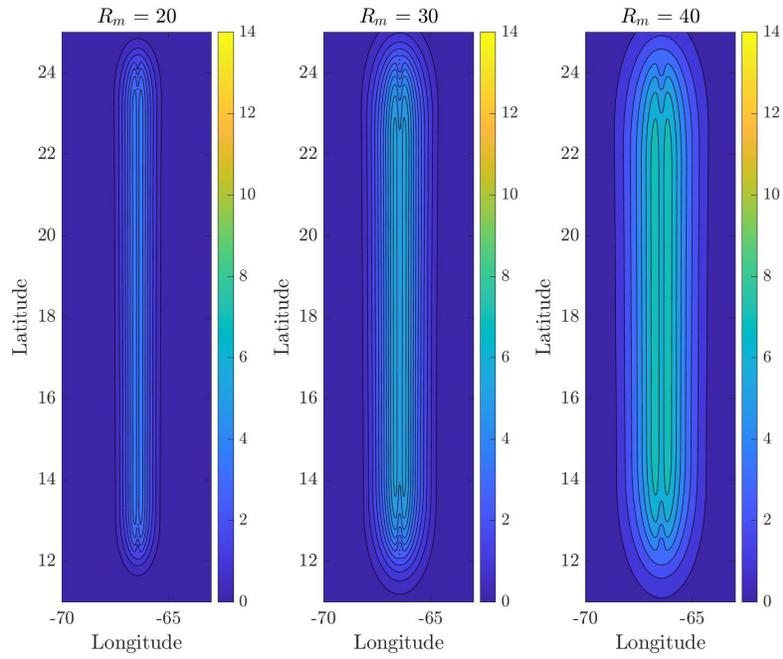
Figure 4: As in Figure 3, but for different values of the radius of maximum winds R_m, with V_m fixed to 37 m s^{-1}.
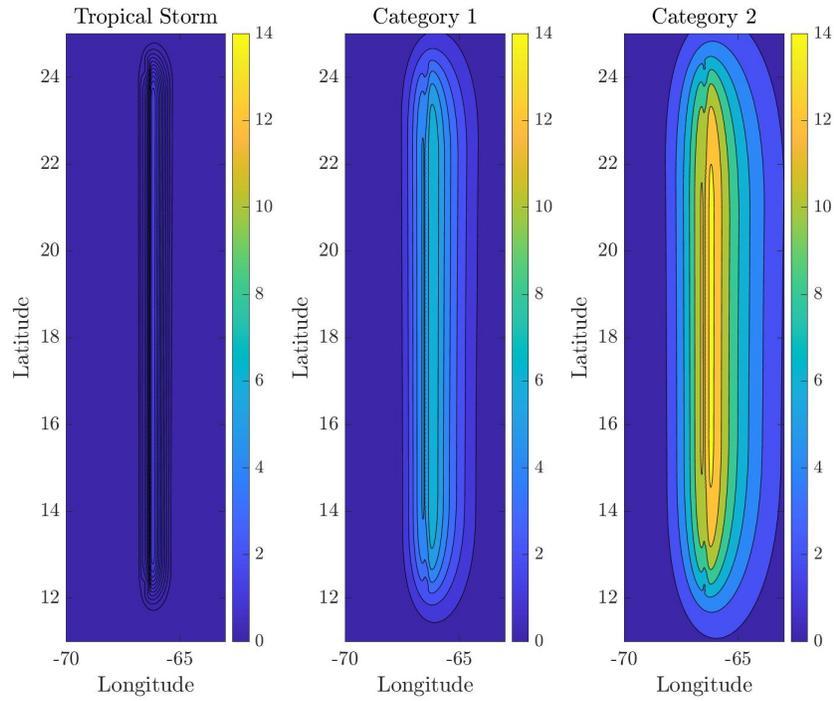
Figure 5: As in Figure 3, but under inclusion of asymmetry due to the storm-translation vector.
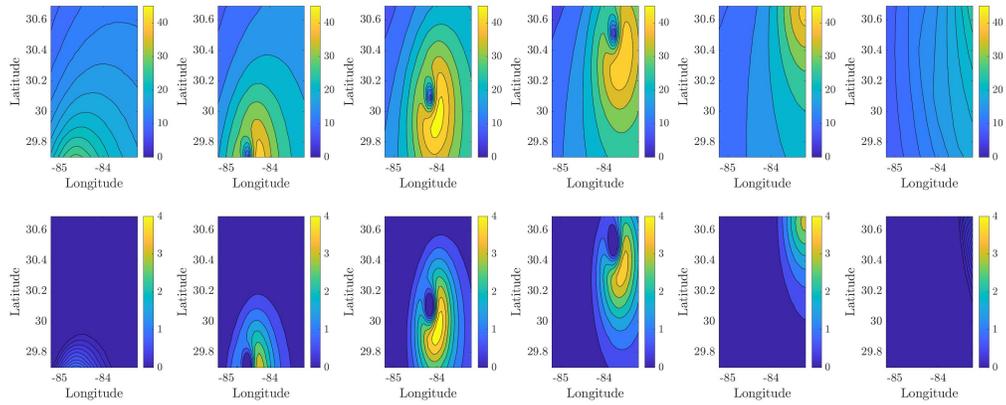
Figure 6: Plot of Hurricane Hermine wind velocities (*top row*) and corresponding Poisson intensities (*bottom row*) for a single ensemble member. Each of the six columns corresponds to a specific time, given in Coordinated Universal Time (UTC).
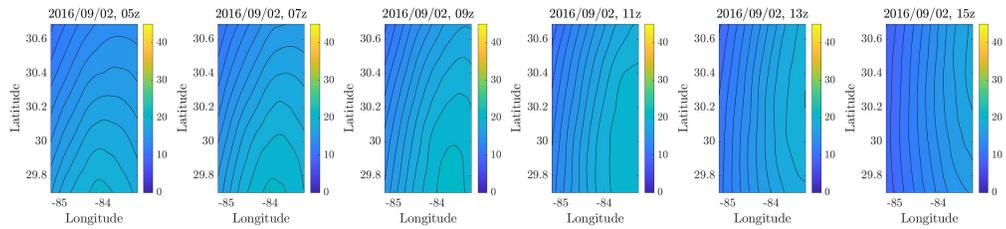

Figure 7: Plot of Hurricane Hermine's velocities averaged across all ensemble members.
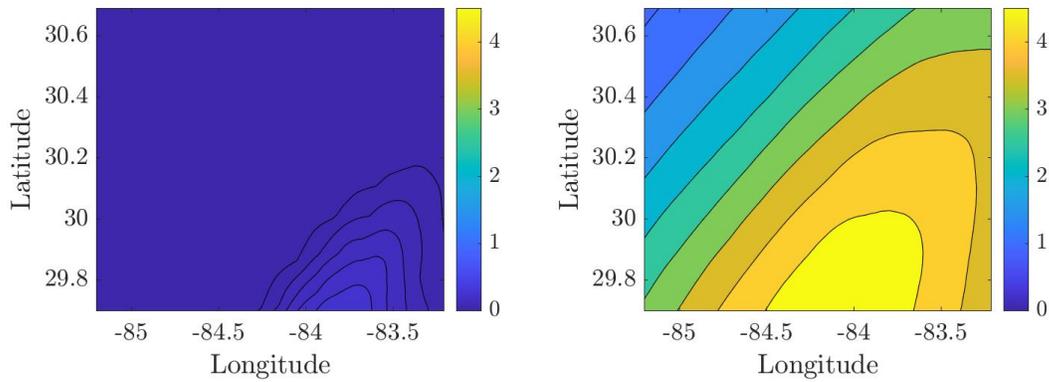
Figure 8: Plot of failure rates given by FR-1 (*left*) and FR-2 (*right*) for Hurricane Hermine.
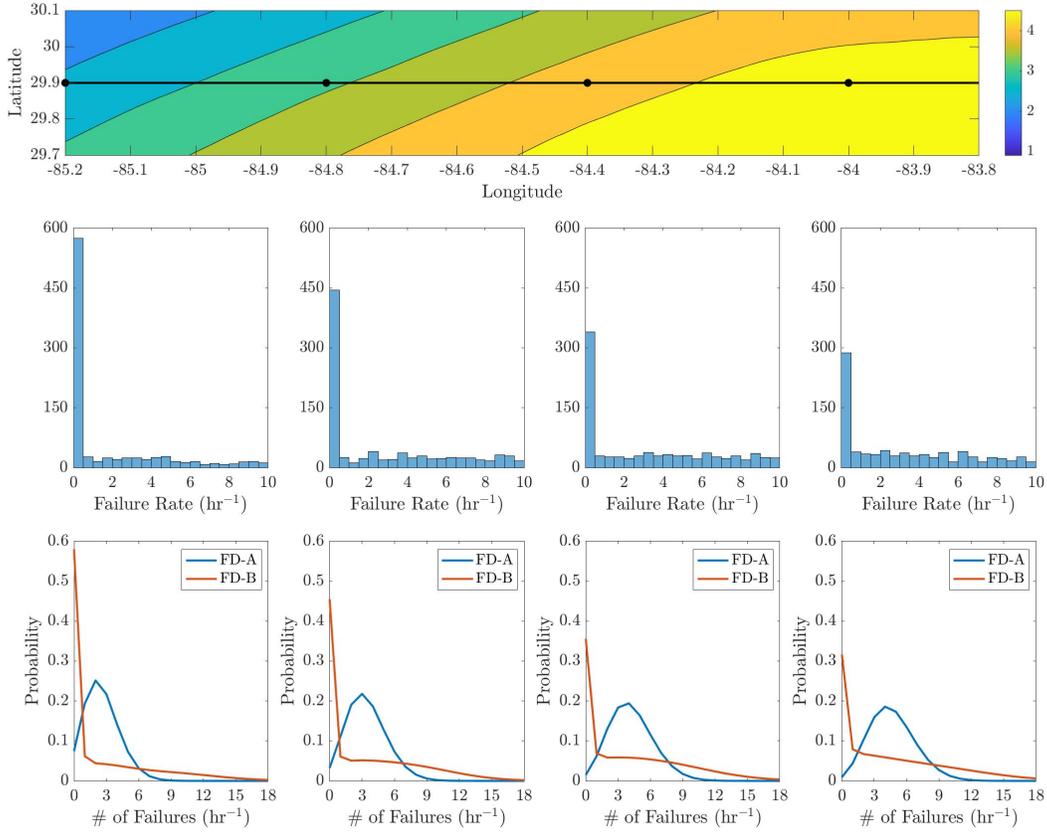
Figure 9: Illustration of how the probability distribution over number of failures depends on the selected failure distribution (FD-A vs. FD-B) for Hurricane Hermine. *Top row*: contour plot of spatially-varying failure rates given by FR-2 or $\mathbb{E}[\Lambda_g(\mathbf{H}_g)]$, with four locations g for analysis marked by the black dots. *Middle row*: Histogram of ensemble member failure rates $\Lambda_g^{(i)}$ at the four identified locations. *Bottom row*: Corresponding probability distributions over number of failures.
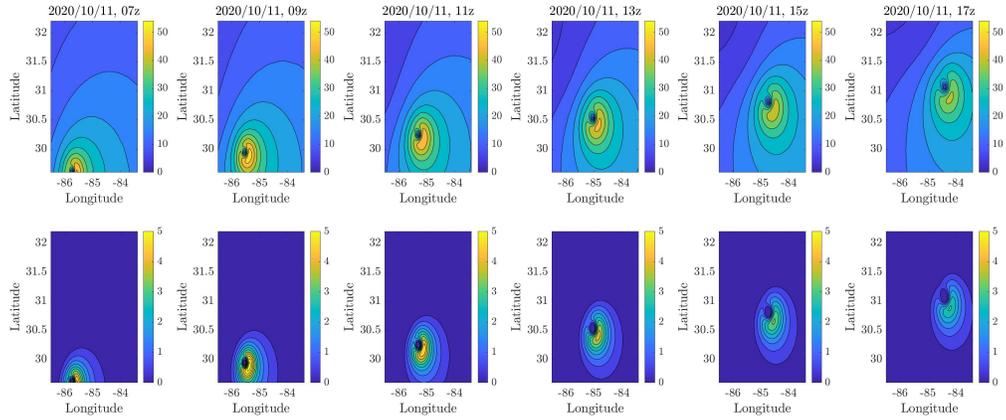
Figure 10: Plot of Hurricane Michael wind velocities (*top row*) and corresponding Poisson intensities (*bottom row*) for a single ensemble member. Each of the six columns corresponds to a specific time, given in Coordinated Universal Time (UTC).
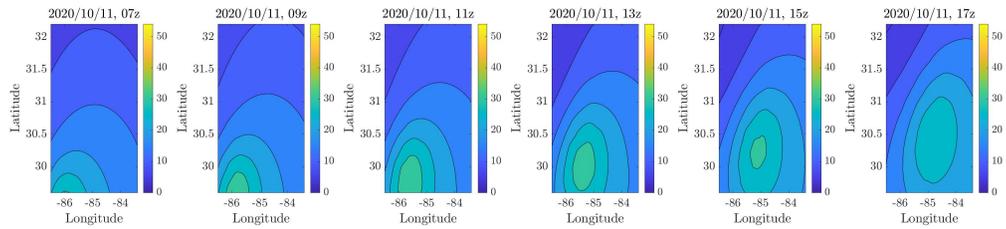
Figure 11: Plot of Hurricane Michael's velocities averaged across all ensemble members.
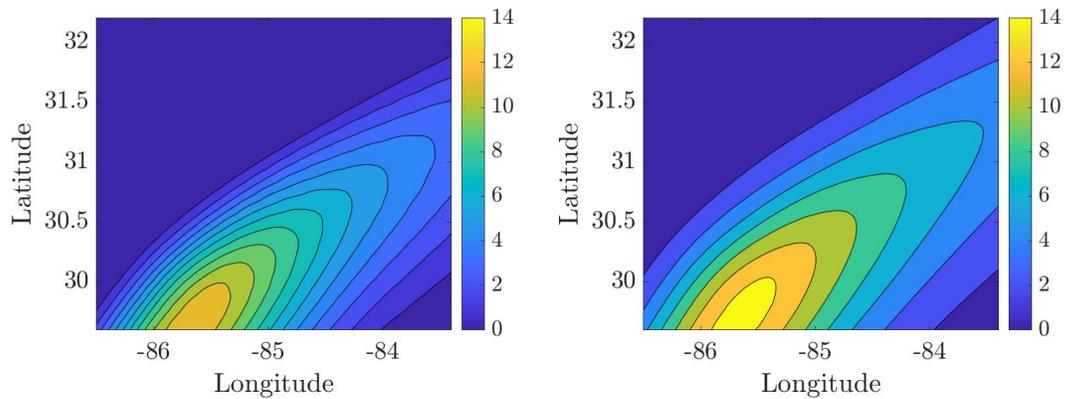

Figure 12: Plot of failure rates given by FR-1 (*left*) and FR-2 (*right*) for Hurricane Michael.
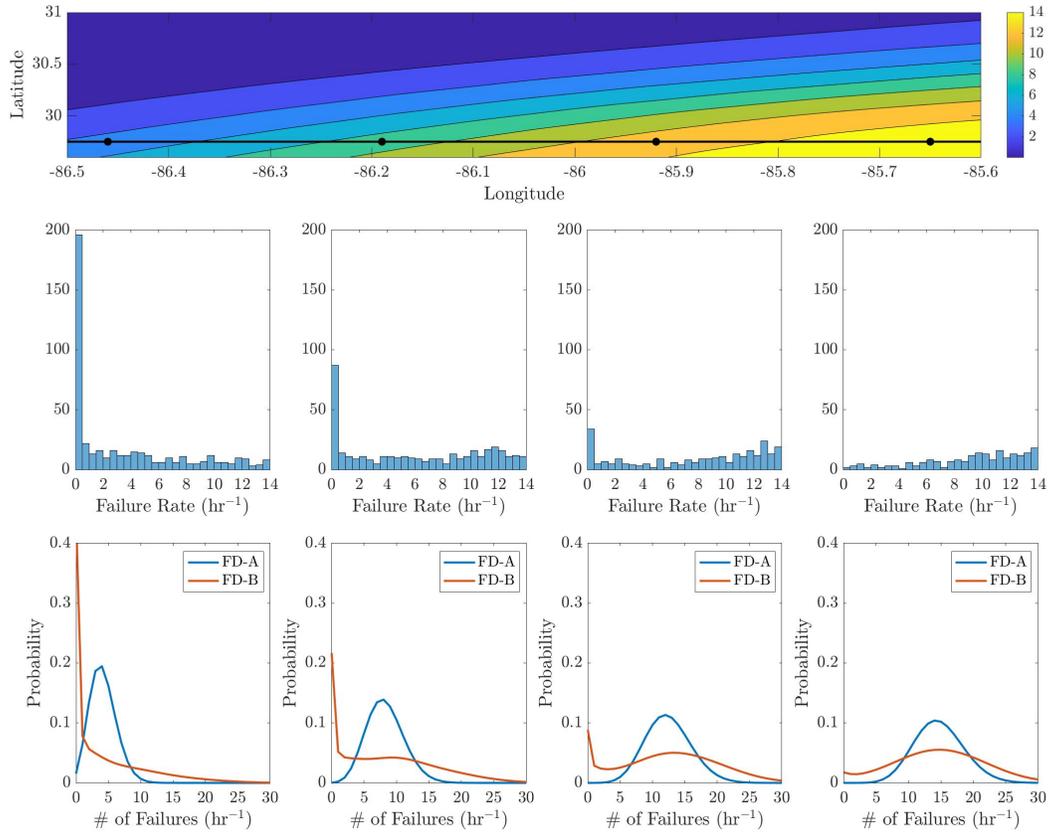
Figure 13: As in Figure 9, but for Hurricane Michael.

(a) October 10, 16:35

(b) October 10, 19:50

(c) October 11, 19:40

(d) October 11, 22:00
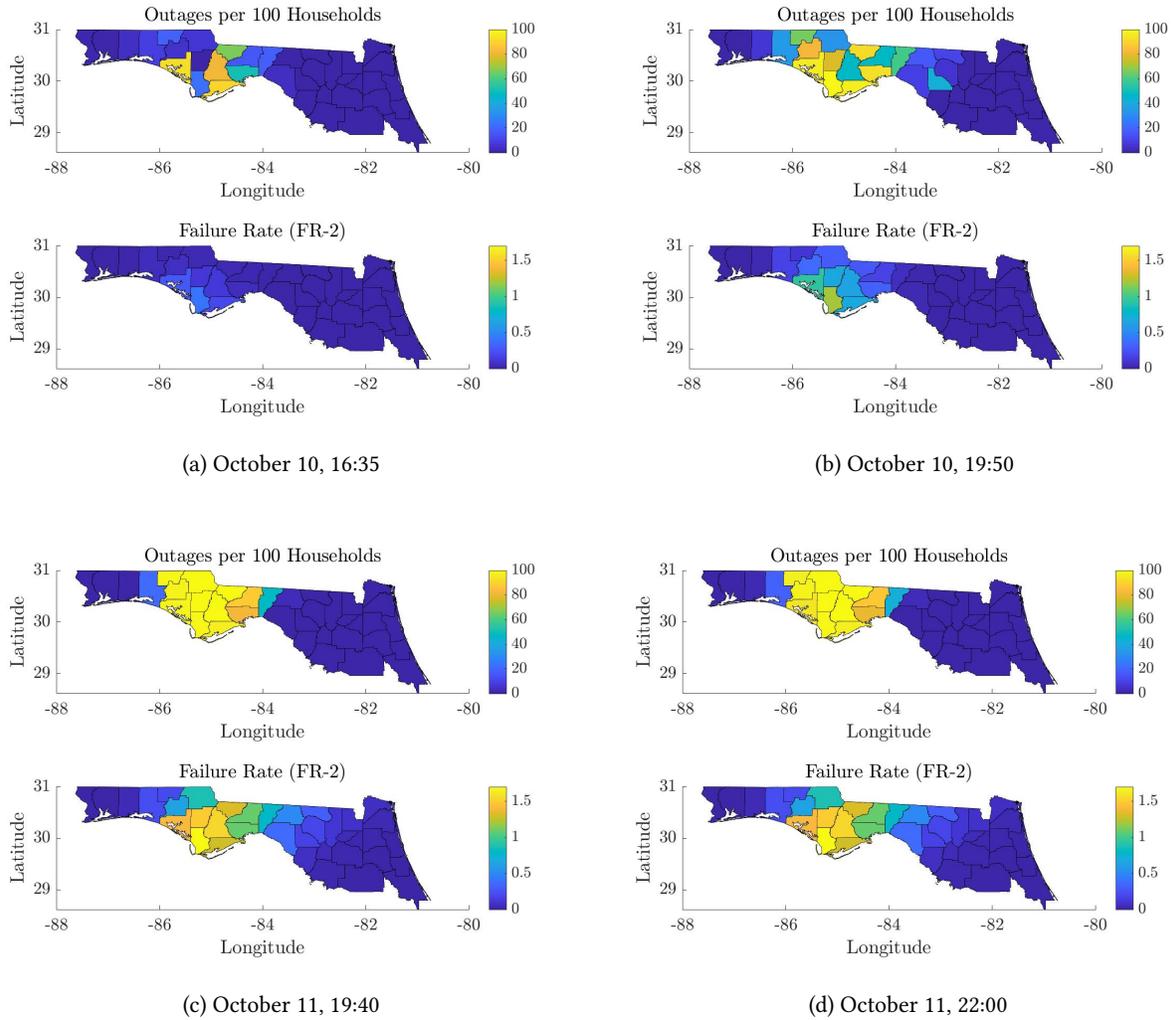
Figure 14: Comparison of outage rates and failure rates (FR-2) in Northern Florida for Hurricane Michael, at four different times after landfall. The outage rate for each county is given by outages per 100 households. The failure rate in each county at a given time is obtained by accumulating Poisson intensities estimated using FHLO from 10/9/2018 at 12Z (7:00am in Florida) to the time in question.
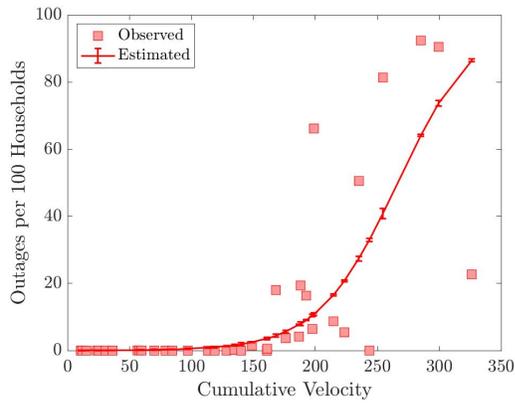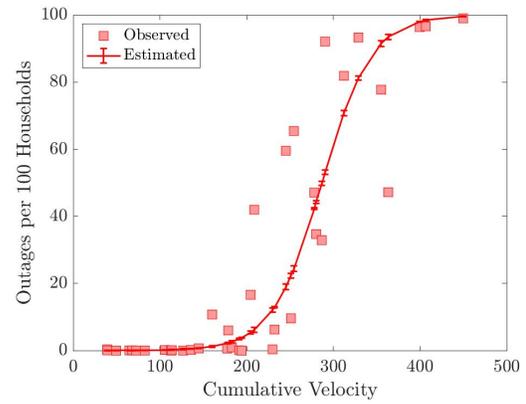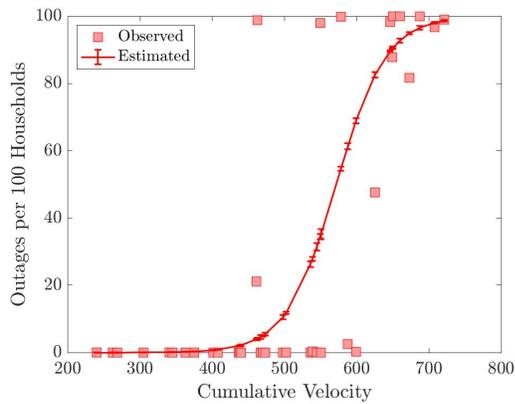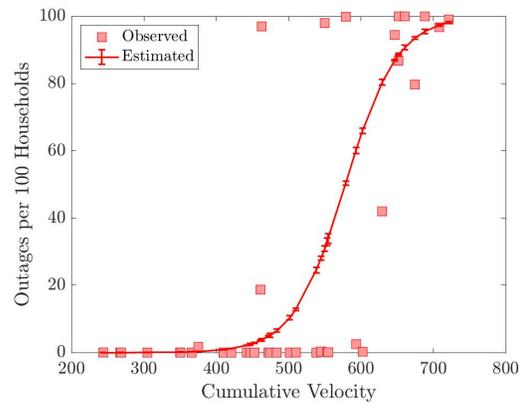
Figure 15: Scatterplots of outages vs. cumulative velocity in Northern Florida for Hurricane Michael, at four different times, accompanied by corresponding estimated binomial regression models. Outages are measured by households without power. The cumulative velocity in a county at a given time is obtained by accumulating velocities estimated using FHLO from 12Z (7:00 in Florida) to the time in question, and then taking the cumulative velocity averaged across all $0.01° \times 0.01°$ grids in the county.
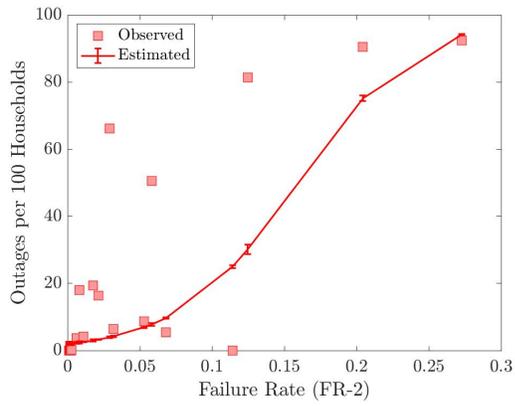
(a) October 10, 16:35
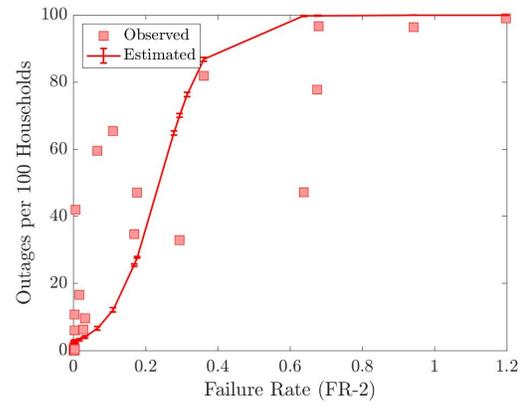
(b) October 10, 19:50
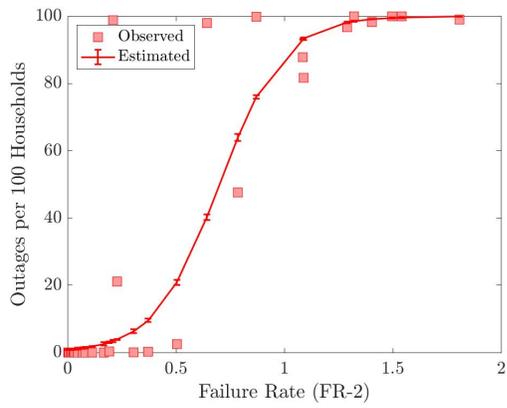
(c) October 11, 19:40
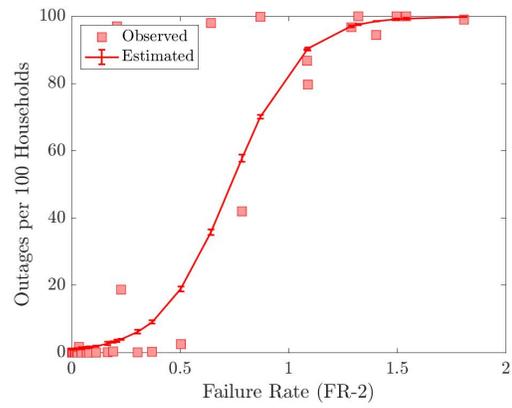
(d) October 11, 22:00

Figure 16: As in Figure 15, but for outages vs. failure rates.
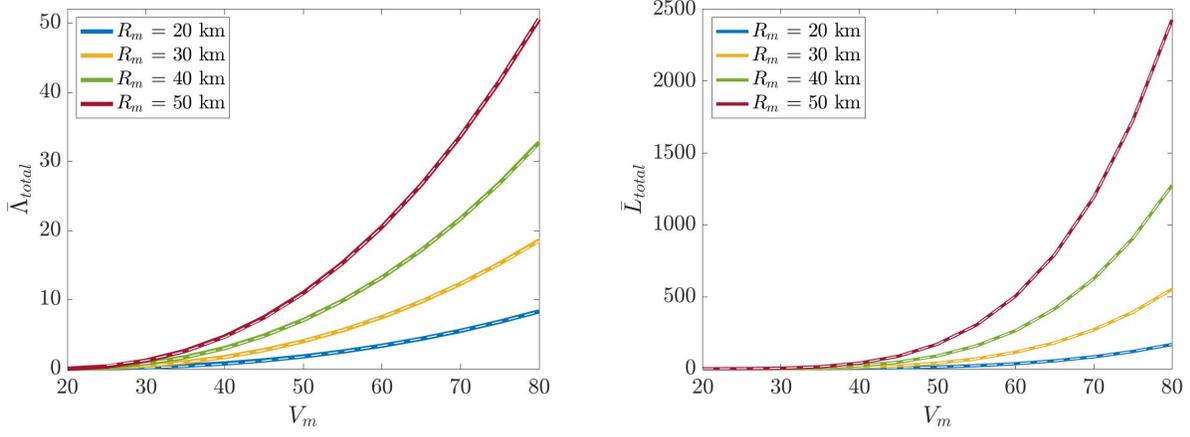
Figure 17: Normalized expected damage $\bar{\Lambda}_{\text{total}}$ (*left*) and expected loss $\bar{L}_{\text{total}}$ (*right*) as a function of V_m for fixed values of R_m. The estimated parametric functions are denoted by the white dotted lines. The numerically-computed values of $\bar{\Lambda}_{\text{total}}$ and $\bar{L}_{\text{total}}$ are given by the dark-colored lines (see Appendix D.2 and E.3 for details).

A Proof of Proposition 2.1

We restate Proposition 2.1 – for a location g and wind velocities $\mathbf{H}_g$, the following holds for the failure rate Λ_g:

$$\mathbb{E}[\Lambda_g(\mathbf{H}_g)] \geqslant \Lambda_g(\mathbb{E}[\mathbf{H}_g]). \tag{23}$$

Proof. First, we show that the following inequality holds:

$$\mathbb{E}[f^2(v_{g,t})] \geqslant f^2(\bar{v}_{g,t}). \tag{24}$$

To do so, we restate the term $f^2(\bar{v}_{g,t})$ following Eq. (6):

$$f^2(\bar{v}_{g,t}) = \begin{cases} 1, & \text{for } \bar{v}_{g,t} < \mathrm{V}_{\mathrm{crit}} \\ \left(\frac{\bar{v}_{g,t}}{\mathrm{V}_{\mathrm{crit}}}\right)^2, & \text{for } \bar{v}_{g,t} \geqslant \mathrm{V}_{\mathrm{crit}} \end{cases} \tag{25}$$

We can note from Eq. (25) that:

$$\frac{\bar{v}_{g,t}^2}{\mathrm{V}_{\mathrm{crit}}^2} \geqslant f^2(\bar{v}_{g,t}). \tag{26}$$

Because $f(v_{g,t}) = \max(\mathrm{V}_{\mathrm{crit}}, v_{g,t})/\mathrm{V}_{\mathrm{crit}}$, it follows that $f(v_{g,t}) \geqslant v_{g,t}/\mathrm{V}_{\mathrm{crit}}$ and $f(v_{g,t}) \geqslant 1$. Then, we obtain the following:

$$\mathbb{E}[f^2(v_{g,t})] \geqslant \frac{\mathbb{E}[v_{g,t}^2]}{\mathrm{V}_{\mathrm{crit}}^2} \geqslant \frac{\bar{v}_{g,t}^2}{\mathrm{V}_{\mathrm{crit}}^2} \tag{27}$$

The right-hand inequality in Eq. (27) is a consequence of Jensen's inequality, noting that $v_{g,t}^2$ is a quadratic function and therefore convex.

From Eq. (26)-(27), we conclude that Eq. (24) holds. Using Eq. (11) and Eq. (13), we arrive at Eq. (23). $\square$

B Estimation of Critical Radius and Critical Zone Area

We demonstrate how the critical radius $\mathrm{R}_{\mathrm{crit}}$ and critical zone area $\mathrm{A}_{\mathrm{crit}}$ vary with the hurricane parameters V_{m} and R_{m}, using the simple hurricane outlined in Section 3.1. Because of the Holland model's inherent nonlinearity, it is difficult to analytically determine $\mathrm{R}_{\mathrm{crit}}$ as a function of the Holland parameters. However, we can obtain an approximate estimate of $\mathrm{R}_{\mathrm{crit}}$ by first defining the 'normalized' critical radius $r_{\mathrm{norm}}^{\star}$:

$$r_{\mathrm{norm}}^{\star} = \frac{\mathrm{R}_{\mathrm{crit}}}{\mathrm{R}_{\mathrm{m}}}. \tag{28}$$

Because Eq. (28) suggests that R_{crit} varies linearly with R_m, we consider a function of the following form for R_{crit}:

$$R_{crit}(V_m, \; R_m) \;=\; \begin{cases} 0 & V_m < V_{crit} & \text{(29a)} \\[2ex] a_1 R_m (V_m/V_{crit})^{a_2} & V_m \geqslant V_{crit}. & \text{(29b)} \end{cases}$$

We obtain Eq. (29a) by noting that $R_{crit}/R_m = 0$ when $V_m < V_{crit}$. We obtain Eq. (29b) by observing that R_{crit}/R_m = 1 for $V_m = V_{crit}$ and increases with V_m for $V_m > V_{crit}$.

Using Lemma 3.3, we arrive at an equation for the critical zone area A_{crit} as a function of R_m and V_m, when $V_m \geqslant V_{crit}$:

$$\begin{aligned} A_{crit}(V_m, \; R_m) \;&=\; 2R_{crit}T\left\|V_{tr}\right\|_2 + \pi R_{crit}^2 \\[1ex] &=\; 2T\left\|V_{tr}\right\|_2 a_1 R_m \left(\frac{V_m}{V_{crit}}\right)^{a_2} + \pi a_1^2 R_m^2 \left(\frac{V_m}{V_{crit}}\right)^{2a_2} \qquad \text{(30)} \\[1ex] &=\; b_1 R_m \left(\frac{V_m}{V_{crit}}\right)^{a_2} + b_2 R_m^2 \left(\frac{V_m}{V_{crit}}\right)^{2a_2}, \end{aligned}$$

where $b_1 = 2T\left\|V_{tr}\right\|_2 a_1$ and $b_2 = \pi a_1^2$. The complete defined parametric function for A_{crit} is as follows:

$$A_{crit}(V_m, \; R_m) \;=\; \begin{cases} 0 & V_m < V_{crit} & \text{(31a)} \\[2ex] b_1 R_m (V_m/V_{crit})^{a_2} + b_2 R_m^2 (V_m/V_{crit})^{2a_2} & V_m \geqslant V_{crit}. & \text{(31b)} \end{cases}$$

For purposes of estimating the parameters a_1 and a_2, we calculate the critical radius numerically for hurricanes with values of R_m between 20 and 50 km (step size of 1 km) and V_m between 21 and 80 m/s (step size of 1 m/s). These hurricanes have a straight-line track moving northward with a lifetime $T = 121$ and translation speed $\left\|V_{tr}\right\|_2 = 3$ m s^{-1}. Then, we take the logarithm of Eq. (29a) and use the least-squares method to estimate the parameters relating V_m and R_m to the critical radius. The resulting parameters, $a_1 = 11.29$ and $a_2 = 3.24$, are statistically significant with 95% confidence (see Figure 1).

C   Binomial Regression Model

The binomial regression model (BRM) is a specific type of generalized linear model (GLM), which is a generalization of ordinary linear regression models that allows for response variables to have non-Gaussian error distribution models. In the BRM, model inputs are used to estimate the probability associated with a Bernoulli trial. Then, this probability estimate is used as a parameter in the binomial distribution, which provides probabilities over the number of outages given a specified number of Bernoulli trials (number of households). The model inputs we consider are

the cumulative velocity $\mathcal{V}$ or failure rate Λ.

The binomial distribution is stated as follows for our problem:

$$\Pr(o_{c,t} \mid \mathbf{x}_{c,t}) \;=\; \binom{nh_c}{o_{c,t}} (\pi_{c,t})^{o_{c,t}} (1 - \pi_{c,t})^{nh_c - o_{c,t}} \tag{32}$$

which predicts the probability that $o_{c,t}$ households suffer from outages at time t and county c, given the input $\mathbf{x}_{c,t}$, single-household outage probability $\pi_{c,t}$, and number of households nh_c. The probability $\pi_{c,t}$ is determined using a generalized linear model (GLM) equation:

$$g(\pi_{c,t} \mid \mathbf{x}_{c,t}) \;=\; \beta_0^{(\mathbf{x},t)} + \beta_1^{(\mathbf{x},t)} \mathbf{x}_{c,t}, \tag{33}$$

where $\mathbf{x}_{c,t}$ is given by the failure rate $\Lambda_{c,t}$ or cumulative velocity $\mathcal{V}_{c,t}$ calculated at time t and for county c, and $g(\cdot)$ is given by the logistic (logit) linking function:

$$g(\pi_{c,t}) \;=\; \ln\left(\frac{\pi_{c,t}}{1 - \pi_{c,t}} \right). \tag{34}$$

Our goal is to estimate the coefficients of the GLM equation, $\beta_0^{(\mathbf{x},t)}$ and $\beta_1^{(\mathbf{x},t)}$, under each choice of input $\mathbf{x}$ (failure rate or cumulative velocity) and at each time t. In order to estimate the coefficients, we use the MATLAB function `glmfit`.

D   Total Damage Dependency on Hurricane Intensity and Size

Throughout the section, we assume equal asset density in all considered locations $g \in \mathcal{G}$.

D.1   Analytical Solution for Total Damage

For the purpose of formulating an equation for total expected damage, let $\mathcal{G}_c$ denote the set of grids that lie inside the critical zone and $\mathcal{G}_u = \mathcal{G} \backslash \mathcal{G}_c$ the set of grids outside the critical zone. Furthermore, we assume that velocities are measured at a discrete set of times $\mathcal{T}$. For a grid g, $\mathcal{T}_{c,g}$ is the set of times for which $v_{g,t} \geqslant V_{\mathrm{crit}}$ and $\mathcal{T}_{u,g} = \mathcal{T} \backslash \mathcal{T}_{c,g}$ is the set of times for which $v_{g,t} < V_{\mathrm{crit}}$. We define $T_{c,g}$ to be the total duration of time during which $v_{g,t} \geqslant V_{\mathrm{crit}}$ and $T_{u,g} = T - T_{c,g}$ to be the total duration of time during which $v_{g,t} < V_{\mathrm{crit}}$.

Then the expected damage in a region (per unit of length of assets) is given by Λ_{total}:

$$\Lambda_{\text{total}} \;=\; \sum_{g \in \mathcal{G}} \Lambda_g \tag{35a}$$

$$=\; \sum_{g \in \mathcal{G}} \left[\lambda_{\text{norm}} \mathrm{T}(1-\alpha) \;+\; \lambda_{\text{norm}} \alpha \Delta t \sum_{t \in \mathcal{T}} f^2(v_{g,t}) \right] \tag{35b}$$

$$=\; |\mathcal{G}| \lambda_{\text{norm}} \mathrm{T}(1-\alpha) + \lambda_{\text{norm}} \alpha \Delta t \sum_{g \in \mathcal{G}} \sum_{t \in \mathcal{T}} f^2(v_{g,t}) \tag{35c}$$

$$=\; |\mathcal{G}| \lambda_{\text{norm}} \mathrm{T}(1-\alpha) + \lambda_{\text{norm}} \alpha \sum_{g \in \mathcal{G}} \left(\mathrm{T}_{u,g} + \sum_{t \in \mathcal{T}_{c,g}} \Delta t f^2(v_{g,t}) \right) \tag{35d}$$

$$=\; |\mathcal{G}| \lambda_{\text{norm}} \mathrm{T}(1-\alpha) + \lambda_{\text{norm}} \alpha \sum_{g \in \mathcal{G}} \left(\mathrm{T} + \sum_{t \in \mathcal{T}_{c,g}} \left(f^2(v_{g,t}) - 1 \right) \Delta t \right) \tag{35e}$$

$$=\; |\mathcal{G}| \lambda_{\text{norm}} \mathrm{T} + \lambda_{\text{norm}} \alpha \sum_{g \in \mathcal{G}_c} \sum_{t \in \mathcal{T}_{c,g}} \left(f^2(v_{g,t}) - 1 \right) \Delta t. \tag{35f}$$

The first term of Eq. (35f) denotes the value of Λ_{total} under nominal conditions; the second term denotes the increase in Λ_{total} due to hurricane winds exceeding the critical velocity V_{crit}.

D.2 Formulation of Parametric Model for Total Damage

We formulate a parametric function for Λ_{total} which accounts for two important considerations. First, we account for the critical velocity V_{crit}, because damage in regions with subcritical winds corresponds to nominal (no-hurricane) damage and is independent of hurricane velocities in the quadratic NHPP model. Second, the total expected damage depends on the area of the critical zone A_{crit}, which is represented by $\mathcal{G}_c$ and can be estimated using Eq. (31a) in Section 3.1. Regarding the critical zone area, we note that velocity increases with radius r for $r \leqslant \mathrm{R_m}$, and then decreases with r for $r > \mathrm{R_m}$ (see Figure 1b). Consequently, the region of the hurricane surrounding the hurricane center (eye) contains subcritical velocities. However, this region is part of the critical zone as defined in Section 3.1, and thus we need to form a parametric model that corrects for this. Let us consider the following parametric damage function:

$$\bar{\Lambda}_{\text{total}}(\mathrm{V_m}, \mathrm{R_m}) \;=\; \Lambda_{\text{total,nom}} + \Lambda_{\text{total,crit}}(\mathrm{V_m}, \mathrm{R_m}) - \Lambda_{\text{total,inner}}(\mathrm{V_m}, \mathrm{R_m}), \tag{36}$$

where expected normalized damage $\bar{\Lambda}_{\text{total}} = \Lambda_{\text{total}}/|\mathcal{G}|$ refers to the expected number of failures per grid per unit length of assets, and:

$$\Lambda_{\text{total,nom}} = c_1$$

$$\Lambda_{\text{total,crit}}(V_m, R_m) = c_2 R_m [g(V_m)]^{p_1} + c_3 R_m^2 [g(V_m)]^{2p_1} \tag{37}$$

$$\Lambda_{\text{total,inner}}(V_m, R_m) = c_4 R_m [g(V_m)]^{p_2} + c_5 R_m^2 [g(V_m)]^{2p_2},$$

where $\Lambda_{\text{total,nom}} = c_1$ is the intercept term; $\Lambda_{\text{total,crit}}(V_m, R_m)$ is an estimate of damage due to velocity exceedances in the critical zone; and $\Lambda_{\text{total,inner}}(V_m, R_m)$ corrects for the inner hurricane region with subcritical velocities. $\Lambda_{\text{total,crit}}(V_m, R_m)$ contains two terms – the first term is a linear function of R_m and the second is a quadratic function of R_m, which is reflective of Eq. (30). Likewise, the first and second terms of $\Lambda_{\text{total,crit}}(V_m, R_m)$ are respectively functions of $[g(V_m)]^{p_1}$ and $[g(V_m)]^{2p_1}$. The term $\Lambda_{\text{total,inner}}(V_m, R_m)$ has the same structure as $\Lambda_{\text{total,crit}}(V_m, R_m)$. If we wish to obtain the total expected damage Λ_{total}, we simply multiply all estimated coefficients (c_1, c_2, c_3, c_4, c_5) by $|\mathcal{G}|$.

For purposes of estimating Eq. (36), we numerically compute expected damage to overhead assets in electricity infrastructure systems, using the NHPP model with the following parameters: $\lambda_{\text{norm}} = 3.5 \times 10^{-5}$ failures/hr/km, $\alpha = 4175.6$, and $V_{\text{crit}} = 20.6$ m/s (Li et al., 2014). We assume a hurricane of duration $T = 24$ hr and consider a geographical region consisting of $|\mathcal{G}| = 1,000$ grids. The expected damage is calculated under values of R_m between 20 and 50 km (step size of 1 km) and V_m between 21 and 80 m/s (step size of 1 m/s). Then to estimate Eq. (36), we consider values of p_1 between 1 and 1.5, and values of p_2 between -0.5 and 0.5. For each combination of p_1 and p_2, we estimate the parameters c_1, c_2, c_3, c_4, and c_5 using the least squares method. The best-fitting polynomials are $p_1 = 1.13$ and $p_2 = 0.00$, i.e., no dependency of $\Lambda_{\text{total,inner}}(V_m, R_m)$ on $g(V_m)$. All coefficients except c_5 are statistically significant, so we omit the second term of $\Lambda_{\text{total,inner}}(V_m, R_m)$ from the final parametric equation. The accompanying best-fitting coefficients are: $c_1 = -2.65 \times 10^{-1}$, $c_2 = 6.70 \times 10^{-3}$, $c_3 = 1.80 \times 10^{-3}$, $c_4 = -9.10 \times 10^{-3}$.

D.3 Incorporating Saturation

Now we compute expected normalized damage $\bar{\Lambda}_{\text{total}}$ under the assumption of finiteness in the number of assets. Figure 2 illustrates the expected normalized damage in a typical rural area that has about $\bar{S}_g = 6.5$ distribution lines

in each spatial location $g \in \mathcal{G}$.[12] The plots of $\bar{\Lambda}_{\text{total}}$ vs. V_m in the left-hand figure feature an S-shaped curve that is similar to what we observed in Figure 17, under $R_m = 30, 40,$ or 50 km. For $R_m = 20$ km, the S shape is less pronounced, but the expected normalized damage still asymptotically approaches $\bar{S}_g = 6.5$ with sufficiently high V_m. In the right-hand plot of damage vs. R_m and V_m, a large portion of the contour plot has a value of 6.5, indicating the saturation.

In Figure 3, we plot $\bar{\Lambda}_{\text{total}}$ in a typical urban area that has about 71 lines per km^2 of area.[13] Once again, we see S-shaped curves as we did in the rural area, as well as large regions of saturation in the right-hand plot.

E   Total Financial Loss Dependency on Hurricane Intensity and Size

We can write the total expected financial losses as:

$$L_{\text{total}} = \sum_{g \in \mathcal{G}} L_g(s_g), \tag{38}$$

where $L_g(s_g)$ is the loss in location g as a function of the number of failures s_g.

To determine the relationship between L_g and s_g, we assume that we have an estimate of the financial loss per failed asset per unit time, and that the estimate is constant with time and for all assets. This estimate permits us to compute the financial loss $L_{g,k}$ in each location g at a given time k after repairs have commenced. Then we estimate L_g by integrating $L_{g,k}$ over time up to a defined time horizon, at which repairs are assumed to be complete. Because the damaged assets in an infrastructure system are repaired over an extended period of time, certain assets may not be repaired for awhile and thus L_g is expected to be a nonlinear function of damage s_g. Under a repair schedule dictated by the network repair model detailed in Section E.1, $L_{g,k}$ (resp. L_g) scales linearly (resp. quadratically) with the number of failures s_g.

Throughout the section, we assume equal asset density in all considered locations $g \in \mathcal{G}$.

---

[12]We considered Talquin Electric Cooperative in Northwestern Florida. They have about 4,400 km of distribution lines, which provide coverage for about 6700 km^2, averaging to 0.65 km of line/km^2 area (Stocks & Yang, July 29, 2020). Under the assumption that a distribution line is on average 100 meters in length, this averages to 6.5 lines/km^2 area. We assume that each spatial location g has an area of 1 km^2.

[13]We considered The City of Tallahassee Utilities. They have 1,800 km of distribution lines over 255 km^2, averaging to 7.08 km of line/km^2 area (Myers & Yang, July 15, 2020). This averages to about 71 distribution lines per grid.

E.1 Network Repair Model

We assume that the financial loss $L_{g,k}$ in a location (grid) g at a given time k scales linearly with the number of failures:

$$L_{g,k} = L_f kl_{g,k}, \tag{39}$$

where L_f is the estimated financial loss per failed asset per unit time and $kl_{g,k}$ is the number of failures remaining in grid g at time k. There are s_g failures at time $k = 0$ (after the passing of the hurricane), i.e., we assume all failures have occurred by the time the hurricane passes. Due to repairs, $kl_{g,k} \leqslant s_g$ at all times $k > 0$.

In addition, we assume that each grid g has a constant repair rate Y (i.e., Y assets are repaired per unit time). Thus the number of failures remaining to be repaired decreases linearly with time by the rate Y, such that the amount of time needed to repair all failures in a grid is given by $K_g = s_g/Y$:

$$kl_{g,k} = \begin{cases} s_g - Yk & \text{for } 0 \leqslant k \leqslant K_g \\ 0 & \text{for } k > K_g. \end{cases} \tag{40}$$

Under this model, the total loss accrued in grid g is given by:

$$\begin{aligned} L_g &= \int_{k=0}^{K_g} L_f kl_{g,k} dk \\ &= L_f \int_{k=0}^{k=K_g} (s_g - Yk) dk \\ &= \frac{1}{2} \frac{L_f}{Y} s_g^2, \end{aligned} \tag{41}$$

which indicates that the total loss L_g scales quadratically with number of failures s_g.

The model we employ here does not consider the effect of network topology on financial losses (in the case of a networked infrastructure system). A more sophisticated model would consider that financial loss incurred at a given time depends more specifically on the loss-of-service in the infrastructure system, rather than the number of damages. The loss-of-service depends on the locations of the damage, as well as the topological properties if the infrastructure system is networked. A relevant example would be an electricity distribution network. After a hurricane passes, some distribution lines that connect bulk power supplies to end users are damaged, and thus a subset of the end users cannot receive electricity. The distribution lines are then repaired, with the repair rate constrained by the available resources and repair crew capacity. At each time period, a financial loss is incurred,

which corresponds to the cost of repair and the cost of electricity demand not met. Generally speaking, we expect that this financial loss will decrease with each set of repairs, after which more end users receive electricity due to reconnection of loads to bulk power upplies.

E.2 Analytical Solution for Total Financial Losses

We use the network repair model to derive an analytical model of total expected financial losses (per unit of length of assets):

$$
L_{\text{total}} = \frac{1}{2}\frac{L_f}{Y}\sum_{g\in\mathcal{G}} s_g^2 \tag{42a}
$$

$$
= \frac{1}{2}\frac{L_f}{Y}\sum_{g\in\mathcal{G}} \Lambda_g^2 \tag{42b}
$$

$$
= \frac{1}{2}\frac{L_f}{Y}\sum_{g\in\mathcal{G}}\left[\lambda_{\text{norm}}T(1-\alpha) + \lambda_{\text{norm}}\alpha\left(T_{u,g} + \sum_{t\in\mathcal{T}_{c,g}} f^2(v_{g,t})\Delta t\right)\right]^2 \tag{42c}
$$

$$
= \frac{1}{2}\frac{L_f}{Y}\sum_{g\in\mathcal{G}}\left[\lambda_{\text{norm}}T(1-\alpha) + \lambda_{\text{norm}}\alpha\left(T + \sum_{t\in\mathcal{T}_{c,g}} \left(f^2(v_{g,t})-1\right)\Delta t\right)\right]^2 \tag{42d}
$$

$$
= \frac{1}{2}\frac{L_f}{Y}\sum_{g\in\mathcal{G}}\left[\lambda_{\text{norm}}T + \lambda_{\text{norm}}\alpha\sum_{t\in\mathcal{T}_{c,g}} \left(f^2(v_{g,t})-1\right)\Delta t\right]^2 \tag{42e}
$$

$$
= \frac{1}{2}\frac{L_f}{Y}|\mathcal{G}_c|(\lambda_{\text{norm}}T)^2 + \frac{1}{2}\frac{L_f}{Y}\sum_{g\in\mathcal{G}_c}\left[\lambda_{\text{norm}}T + \lambda_{\text{norm}}\alpha\sum_{t\in\mathcal{T}_{c,g}} \left(f^2(v_{g,t})-1\right)\Delta t\right]^2 \tag{42f}
$$

$$
= \frac{1}{2}\frac{L_f}{Y}\left(|\mathcal{G}|(\lambda_{\text{norm}}T)^2 + \sum_{g\in\mathcal{G}_c}\left[2\lambda_{\text{norm}}^2\alpha T\sum_{t\in\mathcal{T}_{c,g}} \left(f^2(v_{g,t})-1\right)\Delta t + (\lambda_{\text{norm}}\alpha)^2\left(\sum_{t\in\mathcal{T}_{c,g}} \left(f^2(v_{g,t})-1\right)\Delta t\right)^2\right]\right) \tag{42g}
$$

$$
= \frac{1}{2}\frac{L_f}{Y}\left(|\mathcal{G}|(\lambda_{\text{norm}}T)^2 + 2\lambda_{\text{norm}}^2\alpha T\sum_{g\in\mathcal{G}_c}\sum_{t\in\mathcal{T}_{c,g}} \left(f^2(v_{g,t})-1\right)\Delta t + (\lambda_{\text{norm}}\alpha)^2\sum_{g\in\mathcal{G}_c}\left(\sum_{t\in\mathcal{T}_{c,g}} \left(f^2(v_{g,t})-1\right)\Delta t\right)^2\right) \tag{42h}
$$

Follow Eq. (42h), the total financial loss under nominal (no-hurricane) conditions is given by

$$
L_{\text{total,nom}} = \frac{1}{2}\frac{L_f}{Y}|\mathcal{G}|(\lambda_{\text{norm}}T)^2. \tag{43}
$$

The remaining terms in Eq. (42h) denote the increase in L_{total} due to hurricane winds exceeding the critical velocity. In particular, the term $(\lambda_{\text{norm}}\alpha)^2\sum_{g\in\mathcal{G}_c}\left(\sum_{t\in\mathcal{T}_{c,g}}\left(f^2(v_{g,t})-1\right)\Delta t\right)^2$ indicates that the location-specific financial loss scales with the wind velocity to the 4th power within the critical zone.

E.3 Formulation of Parametric Model for Total Financial Losses

In order to formulate a parametric model for total financial loss given by L_{total}, we consider the parametric model for damage given by Eq. (36) and the network repair model in Appendix E.1. Specifically, Eq. (36) states that total damage $\Lambda_{total} \sim O(R_m^2 g(V_m)^{2c})$ where c is an arbitrary constant, and Appendix E.1 suggests that financial loss is a quadratic function of damage.

Then, let's consider the following parametric financial loss function:

$$
\begin{aligned}
\bar{L}_{total}(V_m, R_m) \;=\; & d_1 + d_2 R_m [g(V_m)]^{q_1} + d_3 R_m^2 [g(V_m)]^{2q_1} + d_4 R_m^3 [g(V_m)]^{3q_1} + d_5 R_m^4 [g(V_m)]^{4q_1} \\
& + d_6 R_m^2 [g(V_m)]^{q_1} + d_7 R_m^3 [g(V_m)]^{q_1} + d_8 R_m^3 [g(V_m)]^{2q_1} + d_9 R_m^4 [g(V_m)]^{2q_1} \\
& + d_{10} R_m + d_{11} R_m^2 + d_{12} R_m^3 + d_{13} R_m^4
\end{aligned}
\tag{44}
$$

where total expected normalized financial loss $\bar{L}_{total} = L_{total}/|\mathcal{G}|$ refers to the expected financial loss per grid per unit length of assets. We obtain Eq. (44) by taking the square of the function for total expected normalized damage given by Eq. (36) and summing like terms in the resultant expression.

For purposes of estimating Eq. (44), we numerically compute expected financial loss using the NHPP parameters, hurricane duration parameters, and geographical region size given in Appendix D.2. The expected financial loss is calculated under values of R_m between 20 and 50 km (step size of 1 km) and V_m between 21 and 80 m/s (step size of 1 m/s). Then to estimate Eq. (44), we consider values of q_1 between 1.2 and 2. For each considered value of q_1, we estimate the parameters d_1 to d_{13} using the least squares method. The best-fitting polynomial degree is $q_1 = 1.88$, and the corresponding statistically significant coefficients are: $d_2 = 1.52 \times 10^{-2}$, $d_4 = 6.42 \times 10^{-6}$, $d_7 = 6.41 \times 10^{-5}$, $d_8 = 3.53 \times 10^{-4}$, $d_9 = -7.54 \times 10^{-7}$.

Unlike previous work on financial loss modeling (Nordhaus, 2006), we can also incorporate saturation into both the damage and financial loss estimation. This would entail using Eq. (4) for the purpose of numerically computing the total expected damage. Then, we could estimate sigmoid functions that relate total damage and financial losses to the storm parameters V_m and R_m.
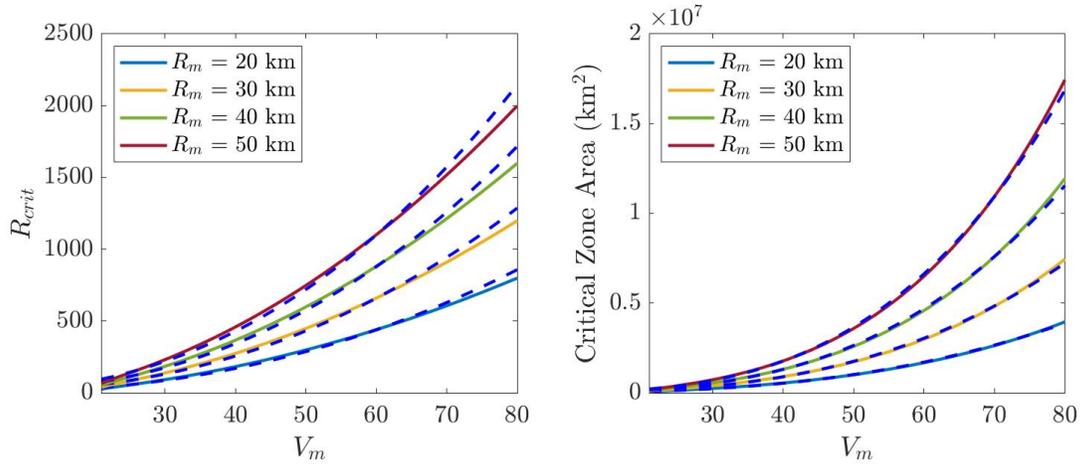
Figure 1: Numerically-computed critical radius R_{crit} (*left*) and critical zone area A_{crit} (*right*), as a function of V_m for fixed values of R_m. Best-fit polynomial functions are included for each curve in both plots, given by the dotted blue lines.
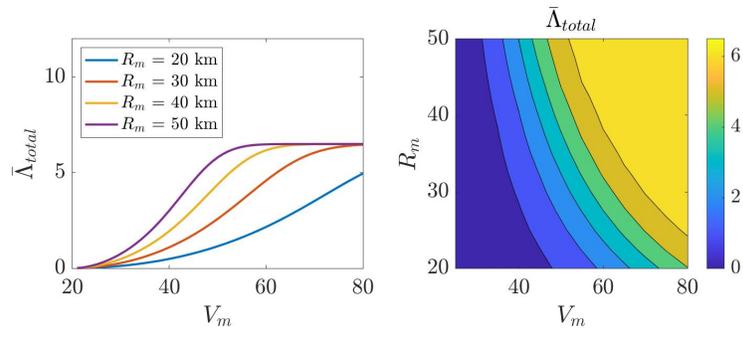
Figure 2: Expected normalized damage $\bar{\Lambda}_{\text{total}}$ in a typical rural area, under the saturation model. *Left*: $\bar{\Lambda}_{\text{total}}$ vs. V_m, under four different values of R_m. *Right*: $\bar{\Lambda}_{\text{total}}$ as a function of both V_m and R_m.
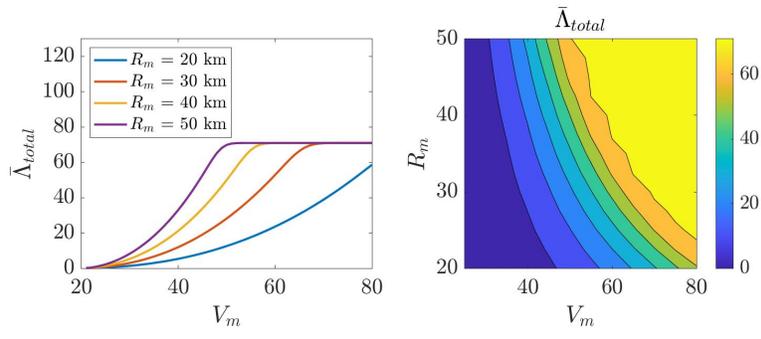
Figure 3: As in Figure 2, but for a typical urban area.